CARAVEL

Publish open access at Caravel Press

Green Technology & Innovation

Journal homepage: gtijournal.com

Technical article

Triggering Mechanisms and Crystallisation Kinetics in Binary Supercooled Sugar-Alcohol Phase Change Materials

Hasila Jarimi [1,2]*, Ze Liu [1] and Yuehong Su [1]

[1] *Department of Architecture and Built Environment, University of Nottingham, Nottingham NG7 2RD, United Kingdom.*
[2] *Solar Energy Research Institute, Universiti Kebangsaan Malaysia, 43600 Bangi, Selangor, Malaysia.*

ABSTRACT

The transition to low-carbon heating in the UK requires large-scale electrification of space and water heating, supported by compact and flexible thermal storage to balance variable renewable electricity supply and heat demand. This work investigates a binary sugar-alcohol–based supercooled phase change material (PCM) as a controllable thermal battery for low-temperature heating systems. The PCM is designed to melt in the 50–90 °C range, providing useful discharge temperatures for radiators and domestic hot water while exploiting long-duration supercooling for deferred heat release. The study was conducted in three stages. First, material screening was performed using T-history analysis to identify suitable binary sugar-alcohol mixtures with high latent heat, stable supercooling, and peak crystallisation temperatures in the target range. A non-eutectic mixture of xylitol–erythritol (Xy–Er) was selected, delivering a cumulative enthalpy of ~287.78 kJ kg^{-1} under triggered conditions while remaining stably supercooled after cooling to ambient. Second, four triggering strategies were systematically evaluated, namely seeding, localised cooling using a thermoelectric (TEC) heat sink, electrode-based activation, and mechanical agitation, including the effect of prior cold crystallisation (reheating to 60 °C). Third, in situ crystallisation image-processing analysis was combined with an Avrami-type (JMAK) model with fixed exponent n=0.5 to quantify effective crystallisation kinetics. The results show that mechanical agitation and electrode triggering at 60 °C outperform seeding and TEC-based cooling, with mechanical agitation yielding the highest effective rate parameters. Meanwhile, TEC-based cooling in the present configuration was insufficient to produce significant crystallisation. These findings demonstrate that appropriately screened sugar-alcohol mixtures, combined with practical triggering methods, can enable controllable supercooled PCMs to be used as on-demand thermal batteries for future low-carbon heating systems.

ARTICLE INFO

Article History:
Received: 22 January 2026
Revised: 01 March 2026
Accepted: 07 April 2026

Keywords:
Binary sugar alcohol
Thermal energy storage
Avrami-type relations
Triggering mechanisms.

Article Citation:
Jarimi, H., Liu, Z., & Su, Y. (2026). Triggering Mechanisms and Crystallisation Kinetics in Binary Supercooled Sugar-Alcohol Phase Change Materials. Green Technology & Innovation, 2(1), 149–175.
https://doi.org/10.65582/gti.2026.009

1. INTRODUCTION

Phase Change Materials (PCMs) store and release thermal energy mainly through solid–liquid phase transitions. Some PCMs can remain liquid below their equilibrium freezing point without unintended

* Corresponding author. Email address: hasila.jarimi@nottingham.ac.uk (Hasila Jarimi)

crystallisation, forming a metastable supercooled state. This behaviour is well-demonstrated for sugar-alcohol eutectics such as xylitol/erythritol, which can retain persistent supercooling over extended periods and enable controllable heat retrieval when crystallisation is intentionally initiated (X. Shao, Yang, et al. 2023).

While supercooling can extend the period over which latent heat is "kept in storage," it also makes heat recovery less predictable because crystallisation may not occur at the desired time without a suitable trigger. This unpredictability is widely recognised as a key barrier to reliable thermal energy storage operation, particularly for systems that require controlled and repeatable heat release (Beaupere, Soupremanien & Zalewski 2018). Similar concerns also arise in hydrated-salt PCMs, where supercooling is commonly reported as a practical limitation and motivates material modification approaches (Xu et al. 2017; Xi et al. 2022).

In applications where on-demand energy delivery is required, controllable supercooling is essential. The concept is to maintain the PCM in a stable supercooled liquid state during standby and then initiate crystallisation only when heat release is needed. This relies on metastability and is governed by nucleation and growth processes, meaning that both thermodynamics and nucleation kinetics influence whether crystallisation starts unintentionally or can be triggered reliably (Karthika et al. 2016; Weiss & Jha 2023).Demonstrations at the prototype level show that stable supercooling can be achieved in practice and then activated through a deliberate triggering mechanism to recover latent heat (Englmair et al. 2018).

Although individual PCMs can be promising, binary and ternary mixtures have been widely investigated to tailor melting temperature ranges, energy density, and cycling stability. For sugar alcohols specifically, mixture design has been motivated by the thermal/chemical stability limits of single components and by the opportunity to tune phase-change temperatures for target applications, particularly in the 70–100 °C range (Palomo Del Barrio et al. 2016). Eutectic and multicomponent sugar alcohol systems have also been examined for thermal endurance and reduced degradation rates compared with some single-component counterparts (Nomura et al., 2015) and eutectic sugar alcohols have been explored for building-related thermal storage alongside crystallisation enhancement strategies (Fan et al. 2022). Related eutectic concepts have been demonstrated for other polyols as well, such as the galactitol–mannitol eutectic PCM (Paul, Shi & Bielawski 2015). For eutectic salt-hydrate mixtures, many studies focus on tailoring phase-change temperatures and latent heat for thermal storage; comparatively fewer works address persistent supercooling and controllable triggering as a primary design target, indicating a gap for long-duration controllable supercooling in multicomponent hydrate systems (Kalidasan et al. 2023).

In this study, we investigate binary erythritol/xylitol sugar-alcohol mixtures in both eutectic and non-eutectic compositions to balance energy density, controllable crystallisation, and cycling stability. Persistent supercooling has already been demonstrated for xylitol/erythritol eutectics, including trigger-based heat retrieval, supporting the suitability of this material family for controllable supercooling research (Shao et al. 2023). Building on this foundation, we systematically assess mixture compositions and experimentally evaluate multiple crystallisation initiation approaches, consistent with the major triggering categories reported in the supercooling-triggering literature (Beaupere et al. 2018).

The key contributions of the paper are as follows. First, it aims to overcome material-specific limitations, whereby we have systematically investigated blends of xylitol and erythritol with the objective of enhancing their thermophysical performance, with particular emphasis on peak transition temperature and latent heat capacity (i.e., energy density). These sugar alcohol mixtures were hypothesised to form homogeneous mixtures in which the individual thermal properties of the components, such as latent heat capacity and melting temperature, complement one another and help to balance supercooling stability and storage density. In addition, we evaluated multiple crystallisation techniques to determine their effectiveness in controlling phase transition in the supercooled state.

Building on this, the work contributes to the development of controllably supercooled phase change materials (PCMs) based on sugar alcohols in three main respects. Initially, suitable supercooled sugar alcohol formulations were identified by systematically investigating binary erythritol–xylitol mixtures over both eutectic and non-eutectic composition ranges, with the objective of optimising the compromise between thermal stability, degree of supercooling, and energy storage density. On the basis of this screening, a binary xylitol–erythritol composition has been found to exhibit a comparatively elevated crystallisation onset temperature, increased enthalpy of phase transition, and enhanced supercooling stability relative to the corresponding pure components. Subsequently, crystallisation-triggering strategies have been explored by experimentally evaluating several nucleation initiation methods applied to the selected sugar alcohol mixtures. The crystallisation kinetics associated with the different triggering methods were analysed and compared using

the modified Avrami relations. It should be emphasised, however, that the purpose of this analysis was strictly comparative; accordingly, the resulting Avrami rate constants *(k)* and exponents *(n)* should not be interpreted as intrinsic, sample-specific material parameters.

2. METHODOLOGY

2.1. MATERIAL PREPARATION AND SCREENING

In this study, to estimate the percentage of the eutectic composition for the binary mixture, we have employed the thermodynamic model of Gibbs excess free energy as in (Fan et al. 2022; Lv et al. 2023). As reported in Fan et al. (2022), it has been shown that the phase diagram as a result of the thermodynamic calculations can accurately predict eutectic sugar-alcohol systems with a specific melting point. Meanwhile, for the non-eutectic mixture, several erythritol-xylitol combinations were prepared and evaluated during preliminary trials to identify a composition with stable thermal behaviour suitable for thermal energy storage. It was observed that mixtures with higher xylitol content had difficulty crystallizing upon cooling, leading to inconsistent phase transitions and incomplete solidification. On the other hand, mixtures with excessive erythritol content can crystallise unintentionally and were difficult to manage during cycling. To balance these issues, a 75 wt% erythritol and 25 wt% xylitol composition was selected. This ratio exhibited more controlled and repeatable solidification, with better overall change stability. In the preparation of the mixture, by referring to X. Shao, Chenxu, et al. (2023) the procedure includes first preparing the materials which total 10 g based on the calculation by means of the molar masses of the two components. Next, all the samples were mixed and grinded which followed by melting the mixture. During melting, the mixture was stirred on a hotplate at 200 rpm and then cooled to produce solid samples for testing. In this study, food-grade erythritol and laboratory-grade xylitol from Sigma-Aldrich were used. Detailed material preparation has also been discussed by the current researchers in (Jarimi, Su & Riffat 2026).

2.1.1. TEMPERATURE HISTORY (T-HISTORY) TEST

The temperature profile for the melting and solidification (crystallization) of sugar alcohols and their thermophysical properties have been evaluated based on the temperature-history (T-history) method. Although conventional calorimetric methods using differential scanning calorimetry (DSC) and differential thermal analyses (DTA) are available, they are complex and expensive and often the samples are too small for the supercooled PCMs to even demonstrate its supercooling properties as shown in bulk samples. In addition, the limitation of the test in terms of visual observation also creates additional barriers to the investigation (X. Shao, 2018). The T-history was investigated by recording the temperature profile of the samples during heating and cooling with a reference sample with known heat capacity following the work of (Sandnes & Rekstad 2006). In the setup as presented in Fig. 1a test tube at 3 cm diameter and 2 cm height of sample has been used. It is worth noting that the temperature sensors were fully immersed in the sample and hence minimizing temperature gradients along the axial direction within the sample. During the testing, the temperatures were measured and logged every 5 s.

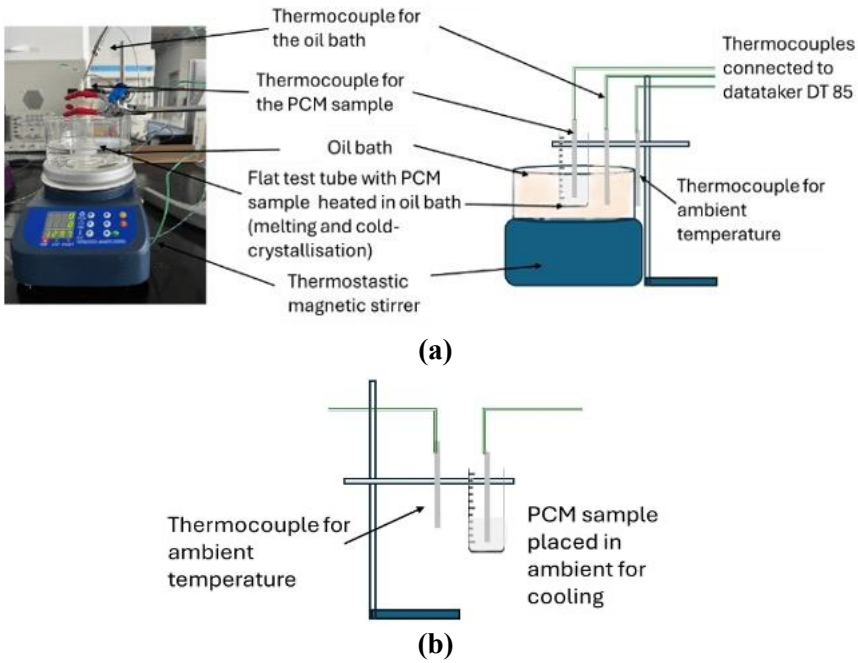

Figure 1. **(a)** Real Setup and schematics for clearer version of the setup during melting, **(b)** the cooling-storage setting.

2.2. TRIGGERING MECHANISMS

As summarised in Table 1, methods for controlled crystallisation generally focus on:

1. Maintaining the supercooled state without premature nucleation and
2. Providing an effective trigger for repeatable initiation.

Reported approaches include nucleating agents, seed-based methods, bubble injection/cavitation-related techniques, and active triggers such as mechanical agitation, thermal triggering, and ultrasound (Beaupere et al. 2018). Beyond lab-scale concepts, electrically triggered crystallisation has also been demonstrated for supercooled sodium acetate trihydrate (SAT) composites, supporting controlled nucleation under defined activation conditions (Chen et al. 2023; Dong et al. 2024). These methods are further detailed in the next sections.

Table 1. Summary of existing research on triggering mechanisms of supercooled PCMs (Jarimi et al. 2025).

Type of triggering	Supercooled PCMs	Trigger Method	Key Results	The fundamental mechanism	Reference
Local cooling	Sodium acetate trihydrate	CO_2 + Peltier cooling	Two series of ten experiments were conducted using the Peltier triggering device. After the SA–water mixture had cooled to ambient temperature, the Peltier device was switched on. The temperature recorded near the lower Peltier element (Tsteel plate) varied between −31 and −36 °C. Despite the limited cooling power of the Peltier elements, the cold side still reached sufficiently low temperatures when the SA–water mixture supercooled to below 30 °C.	Temperature was brought down to crystallisation temperature	Englmair et al. (2018)
Mechanical agitation	Erythritol + nano-Al_2O_3	Nano-assisted nucleation	Enhanced wetting and crystallization capabilities	Cavitation - pressure variation	(Yuan et al. 2021)

Type of triggering	Supercooled PCMs	Trigger Method	Key Results	The fundamental mechanism	Reference
Mechanical agitation	Erythritol/Xylitol	Agitation with seeding	The time for crystallization decreased from 43.3 minutes to 1.8 minutes.	effect when the bubble collapsed.	(X. Shao, Chenxu, et al., 2023)
Bubble injection	Erythritol/Xylitol	MWCNT + bubble injection	Solidification enthalpy = 203.1 J/g, stable over 100 cycles Supercooling reduced by 39.35 °C; enthalpy increased by 50 J/g		(Hou et al. 2023)
Bubble injection	Erythritol	Nitrogen bubble injection	Reduced supercooling to 5 °C; crystallization triggered on demand		(Yang et al. 2022)
Mechanical shock	SAT	Percussion vibration in sealed module	Induction time varies with ball size/position; 2–5 s typical	Vibrations help to refine crystalline particles.	(Zhou, Zhu & Xiang 2018)
Electric and ultrasonic	Water	Ultrasonic waves (45 kHz)	Triggered crystallization observed in controlled conditions	By inducing cavitation.	(Hozumi et al. no date)
Electrical triggering	SAT with Copper Foam/EG	Electric (1.5V DC)	Initiates within 5 seconds; improved thermal conductivity. Crystallization activated in 5-10 seconds; remains stable for over 100 cycles.	Local crystallization induced at the anode via electric field and surface-seeded nucleation	(Dong et al. 2024)
	Sodium acetate trihydrate SAT/CMC/EG	Electric using structured electrodes	Consistent for over 100 cycles, with an induction time of less than 10 seconds		(Chen et al. 2023)
	Sodium acetate trihydrate (SAT)	Electrical activation using graphite cathode and silver anode with surface-treated silver electrode to create nucleation site	Initiating nucleation successfully at approximately 30 °C led to a temperature increase from 29.5 °C to 57 °C when activated with 9 V.		(Kutlu et al. 2023)

2.2.1. SEEDING

The process of seeding is one of the most fundamental methodologies for instigating nucleation in supercooled substances. This process involves the introduction of a stable solid crystal congruent with the material, which serves to expedite the crystallization of the adjacent liquid phase. The resultant structural transformation enhances the stability of the system and facilitates the liberation of latent heat. Due to its reproducibility and efficacy in heat dissipation, seeding has been the subject of extensive empirical investigations. However, a notable challenge associated with seeding is maintaining the persistent availability of solid seed crystals during the melting of the predominant phase change material (PCM). Moreover, the mechanism of 'seeding' introduction itself presents opportunities for various innovations and investigations. For instance, questions arise about whether seeding should be introduced onto the surface of supercooled phase change materials (PCMs), injected into their core, or released concurrently with bubbles. In the current study, as illustrated in Figure 2, seeding was effectively achieved by simply introducing sugar alcohol crystals by injecting them into the core of the PCMs.

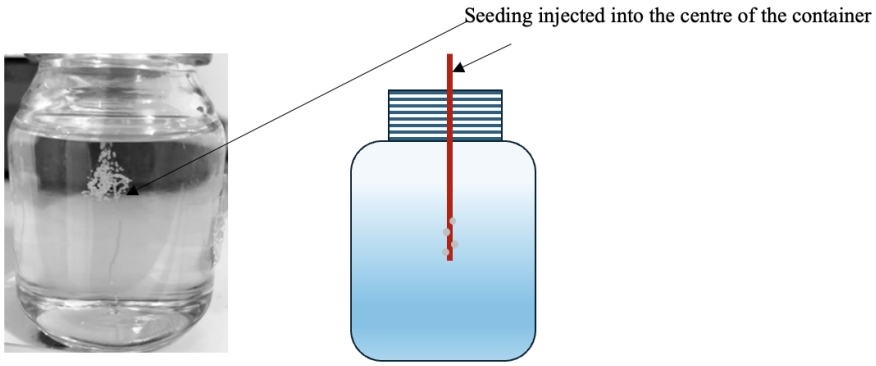

Figure 2. Seeding mechanism representation.

2.2.2. TEC HEAT SINK

The basic process behind nucleation induction through localized cooling is based on starting the nucleation. This start happens when the material's temperature is lowered to its crystallization point, thus creating nucleation sites. Cooling sodium acetate trihydrate (SAT) in its liquid state down to its crystallization temperature can lead to heterogeneous nucleation (Englmair, Jiang, et al. 2018). Therefore, it is understood that localized cooling effectively initiates nucleation when the local temperature reaches the crystallization point. Studies on the effect of localized cooling on supercooled phase change materials (PCMs) have found that local cooling methods, like carbon dioxide evaporation and Peltier modules, are effective in thermally triggering and managing the crystallization process on SAT. As shown in Figure 3, this study uses the TEC Peltier module to provide localized cooling for selected sugar alcohol PCMs to assess its capability in triggering the sample. In this investigation, as depicted in Figure 3, a Peltier cooler was utilized to achieve low temperature to initiate crystallisation in conjunction with a heat sink. Although the Peltier cooler is capable of reaching subzero temperatures, the thermal gain from the surrounding environment and its low capacity limited the heat sink tip to a minimum temperature of approximately 5 °C. In comparison, previous research as in (Englmair, Jiang, et al. 2018), achieved average temperature as low as -31 °C when triggered by the Peltier cooler at high capacity. As a result, crystallisation was observed in their study, highlighting the limitation of the current study.

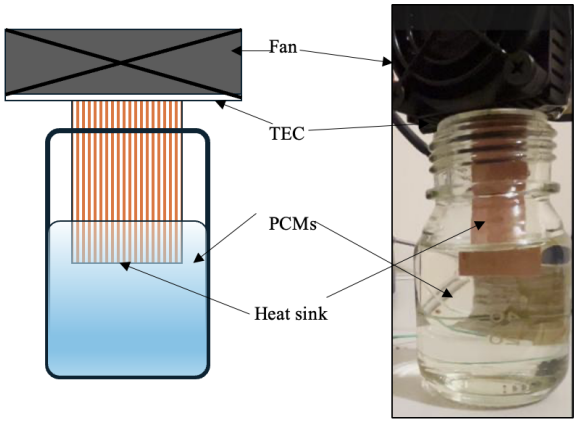

Figure 3. a sketch showing the Peltier cooling crystallisation mechanism using highly efficient heat sink.

2.2.3. ELECTRIFICATION

Meanwhile, for electrical mechanism, among the researchers who investigate the triggering mechanism are (Dong et al. 2024) and (Chen et al. 2023) who applied low-voltage fields (1.0–1.5 V) to crystallize supercooled SAT composites. Dong et al. demonstrated sub-second triggering (0.5 s) with dendritic growth observed, while Chen et al. achieved stable control over 100 cycles using structured electrodes. Despite these advances, surface

degradation and electrode oxidation over time present challenges to durability. Nevertheless, as illustrated in Figure 4, we investigated its potential as a crystallisation mechanism by conducting tests using a pair of cylindrical copper electrodes with a 1 mm diameter under 4.5 V low voltage supply.

Figure 4. A pair of copper electrodes with 4.5 V power supply

2.2.4. MECHANICAL AGITATION

Mechanical agitation in crystallization is a triggering method in which physical disturbance such as stirring, vibration, or bubble injection is applied to a supercooled phase change material to promote nucleation. In this approach, the movement of the liquid and introduction of bubbles or solid seeds create local fluctuations in temperature and structure, breaking the metastable state and providing active sites where crystals can start to form. This enhances the reliability of crystallization, reduces the degree of supercooling, and shortens the time required for the material to solidify. In some systems, mechanical agitation is combined with seeding particles or additives (e.g. nanoparticles) to further stabilise nucleation, although this can introduce practical challenges related to flow control, dispersion, and system sealing in larger-scale applications (Jarimi et al. 2025). In this study, a simple manual stirring procedure was implemented, consisting of continuous agitation for 1 minute for each sample. However, due to the viscosity of the sample at 30 °C, the effective stirring rate for the lower-temperature phase change material (PCM) was reduced by approximately 25%.

2.2.5. COLD CRYSTALLISATION

A review of various triggering methods reported in the literature revealed that, at low temperatures, the crystallization kinetics of the sample are significantly hindered. We therefore propose combining these triggering approaches with a cold-crystallisation method. Cold crystallization denotes an exothermic crystallization process that takes place upon reheating at temperatures below the melting point, allowing the controlled release of stored latent heat from a supercooled PCM. In long-term latent heat storage schemes, the PCM is first charged by melting, then cooled to form a supercooled state for storage, and the stored energy is later extracted by inducing crystallization. A reheating-based thermal triggering strategy (cold-crystallization upon heating) has been shown for supercooled sugar alcohol systems, where crystallization is deliberately activated during the reheating phase instead of during the cooling and storage stage (Puupponen & Seppälä, 2018; Turunen et al., 2023; Yazdani et al., 2020). The cold-crystallisation technique has demonstrated the operational feasibility of thermal energy storage as studied in (Turunen et al. 2023). This level of efficiency is achieved by exploiting the latent heat associated with the phase transition of melting for extended storage durations, and the sensible heat resulting from supercooling for shorter storage periods. The prototype facilitated the determination of a previously unidentified critical cooling rate, above which premature crystallization is inhibited during supercooling, notwithstanding the inherent unpredictability of supercooling and crystallization phenomena (Turunen et al. 2023).

The cold-crystallization process, as illustrated in Figure 5, comprises several steps. Initially, the samples undergo a melting process in an oil bath maintained at 130 °C. Upon complete melting, the samples are subjected to a controlled ambient temperature of 20 °C and subsequently cooled to 30 °C (step 2). At this

cooled state, the samples are in a supercooled state, below their glass transition temperature. The samples were then momentarily pre-heated at the specified rate to the cold-crystallisation temperature (step 3), after which seeding, TEC localised cooling, electrode triggering, or mechanical agitation was introduced to initiate crystallisation. TEC heat sink, Electrode and mechanical agitation was introduced to initiate crystallisation. The momentary heating enhances molecular mobility due to the increased kinetic energy. This kinetic enhancement contributes to the formation of crystal nuclei, a process requiring energy. As crystallization progresses, exothermic heat release reaches a peak, as illustrated in the temperature curve in Figure 5.

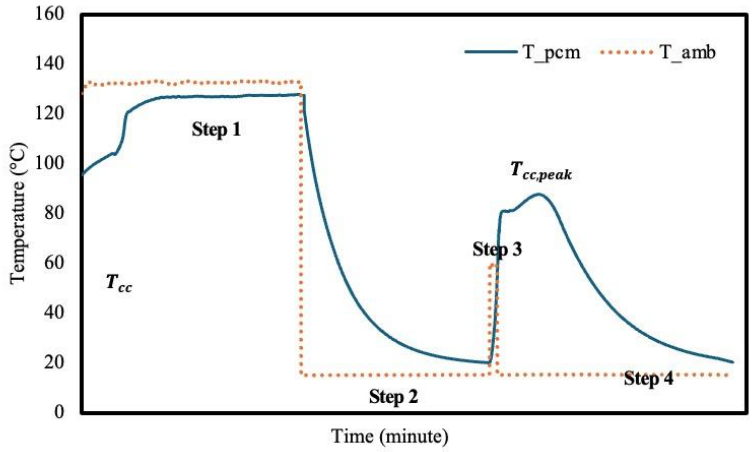

Figure 5. The cold crystallization mechanism.

Subsequently, the samples are exposed to an ambient temperature of 20 °C (step 4). During this phase, the sample temperature rises to reach the peak temperature, and even though crystallization is underway, the rate of heat release diminishes, leading the system to a quasi-stable state. As crystallization nears completion and equilibrium is approached, heat release continues to decrease, resulting in a temperature decline. It is important to note that for samples with a high potential for self-crystallization, the controlled progression of steps 3 and 4 may not be applicable.

2.3. IMAGE-BASED ANALYSIS OF PCM CRYSTALLISATION

Crystallisation of the PCM was monitored using a series of digital photographs acquired at selected times (0, 1, 5, 15, 30 and 40 min), together with a final frame in which the sample appeared fully crystallised. Image processing was performed in MATLAB. First, all images were first converted to grayscale, and a fixed rectangular region of interest (ROI) enclosing the PCM inside the bottle was selected on the initial frame. The same ROI was then applied to all subsequent frames. To compensate for small differences in image resolution between frames, each ROI was cropped and, when required, resized so that all ROIs had identical pixel dimensions.

The first frame, corresponding to the fully liquid state, was taken as the 0% crystallisation reference, $I_0(x,y)$, and the last frame, corresponding to the visually fully crystallised state, as the 100% crystallisation reference, $I_{100}(x,y)$. For each intermediate frame at time t, with grayscale intensity field $I_t(x,y)$, a local crystallisation fraction $f_t(x,y)$ was computed at each pixel by linear interpolation between the two reference states:

$$f_t(x,y) = \frac{[I_t(x,y) - I^0(x,y)]}{[I_{100}(x,y) - I_0(x,y) + \varepsilon]} \quad (1)$$

where ε is a small constant used to avoid division by zero at pixels where the intensity difference between the reference images is negligible. The resulting fraction was clipped to the range $0 \leq f_t(x,y) \leq 1$, such that $f_t = 0$ represents the liquid reference and $f_t = 1$ represents the fully crystallised reference at that pixel. The global crystallised area fraction at each time was then obtained as the spatial average of $f_t(x,y)$ over the ROI and reported as a percentage. Fraction maps were also visualised as colour maps (0–1 scale) overlaid on the grayscale bottle images using a semi-transparent layer, providing a qualitative view of the spatial progression

of crystallisation within the PCM volume.

Furthermore, as an internal consistency check of the image-based method, the fully crystallised reference frame (expected 100%) as shown in Figure 6(a) was quantified as 99.14%, corresponding to a relative error of 0.86%.

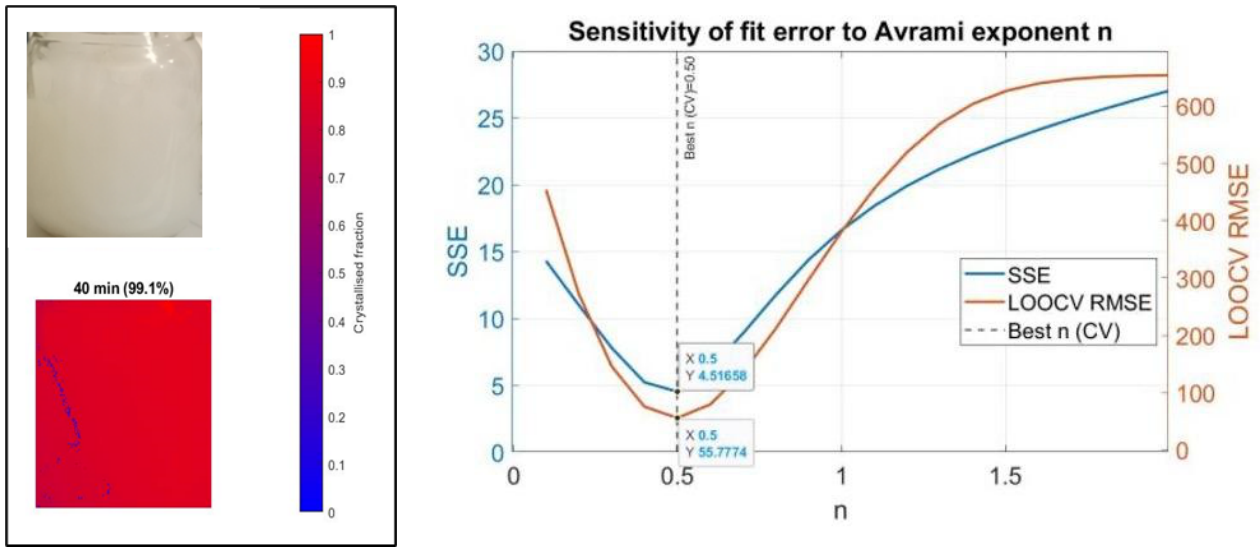

(**a**) (**b**)

Figure 6. **(a)** The fully crystallised frame (expected for 100 % crystallisation) **(b)** The sensitivity analysis for the n-value.

2.3.1. KINETIC CRYSTALLISATION

Avrami-type relations are widely reported for phase-transformation progress curves (Shirzad & Viney 2023), therefore, in this study, we report Avrami-form fits as a benchmark for comparing different triggering mechanisms. The Avrami (Johnson–Mehl–Avrami–Kolmogorov, JMAK) expression is commonly written as:

$$X(t) = 100 \times \left(1 - e^{-kt^n}\right) \quad (2)$$

where $X(t)$ is the fraction of material that is transformed as a function of time, and k and n are constants that are extracted from the model. As discussed in (Shirzad & Viney 2023), it is originated in classical nucleation theory (CNT) and represents the convergence of analyses performed independently by Johnson & Mehl (Johnson, 1939) (Avrami 1940; Avrami 1941). This kinetic analysis clarifies how mixture composition and triggering methodology jointly regulate controllable heat release in supercooled sugar alcohol PCMs. Nucleation arises unintendedly from random fluctuations in the atomic (or molecular) arrangement of the parent phase (Sosso et al. 2016) and occurs in two forms: homogeneous nucleation, in which free-standing nuclei form without external sites, and heterogeneous nucleation, which is assisted by crystal defects or foreign surfaces (Karthika, Radhakrishnan & Kalaichelvi 2016; Callister Jr & Rethwisch 2020). In practical supercooled PCM systems, crystallisation is typically initiated by heterogeneous nucleation on container walls, impurities/particles, or deliberately added nucleation sites (seeds/nucleating agents), while homogeneous nucleation is rarely observed. Therefore, controlled heat release commonly relies on introducing nucleation centres or external triggering methods (e.g., seeding, bubbling/agitation, ultrasonication) to initiate crystallisation on demand (Englmair, Moser, et al. 2018).

Based on the literature, Table 2 summarises studies on polyol-based thermal energy storage systems that employed Avrami-type equations to analyse crystallisation kinetics of the polyols sample. Only two studies were identified on polyol-based PCMs. Note that, in principle, crystallisation of supercooled polyols is non-isothermal due to the release of latent heat and the associated sensible temperature rise. In this work, we nevertheless use Avrami-type correlations, derived for isothermal conditions, as an empirical benchmark to compare crystallisation behaviours. The model is not intended to capture the full non-isothermal thermodynamic coupling, but to provide a consistent phenomenological comparison across different triggering mechanisms with and without cold crystallisation via heating.

Table 2. Summary of polyols based PCM employing Avrami-type relations for kinetic crystallisation research.

PCM system	Crystallisation test	Avrami/JMAK form used	Reported (*n*)	Reported rate constant	Reference
Erythritol in cross-linked sodium polyacrylate ("cold-crystallising material")	Isothermal cold crystallisation at multiple temperatures	$\left(\alpha(t) = 1 - exp(-Kt^n)\right)$	$n = 2.5$ for above the "deeply supercooled" regime; and (n=1.23,1.43,1.52) at 0 °C, 5 °C, 10 °C	Authors fit (K) (temperature-dependent) and discuss the rate constant's temperature dependence (Arrhenius deviation near glass-transition region).	(Turunen et al. 2021)
Erythritol/expanded graphite composite PCM (with nano-particle additive)	Non-isothermal crystallisation at different cooling rates	Modified Avrami (Jeziorny-type) fitting to non-isothermal progress $1 - X(t) = exp(-Zt^n)$; where $Z = \frac{\pi}{3}JK^3$	(*n* = 4.10, 4.12, 4.13, 4.15, 4.22) (for 3, 6, 9, 12, 18 °C/min cooling rate)	Rate constant reported as (G) (min^{-1}): (0.21, 0.51, 0.77, 1.05, 1.75) (for 3, 6, 9, 12, 18 °C/min cooling rate)	(Yuan et al. 2021)

For the present image-based analysis, crystallisation was quantified at discrete times (5, 15, 30 and 40 min). To enable consistent comparison across triggering methods using the same fitting approach, the Avrami exponent n was fixed rather than fitted simultaneously with *k*. In selecting the best n value, we have conducted a sensitivity check for the mechanical agitation crystallisation mechanism as a complete crystallisation was achieved via the triggering method. In order to conduct the sensitivity analysis, the *n* value was varied in the range of 0.1-2 at the interval of 1 decimal point. To conduct the sensitivity analysis, we conducted first Sum of Squared Errors (SSE) given in Equation (3), and to further verify the analysis. However, given the limited number of data we have, we have also employed the leave-one-out cross-validation root-mean-squared error (LOOCV-RMSE) statistical method.

For each simulated *n*, we estimated the LOOCV-RMSE for each model by iteratively omitting one *X*-data point from model fitting, predicting its log-transformed concentration, and computing the difference between observed and predicted values. We then calculated the RMSE as the square root of the mean of these squared differences across all data. Values closer to 0 indicate better model performance, and we ensured the chosen model did not have an excessively large LOOCV-RMSE given the small sample size.

$$SSE = \sum_{i=1}^{n} \left(X_{data} - X_{fit}\right)^2 \tag{3}$$

As illustrated in Figure 6b the best SSE and LOOCV was obtained when $n = 0.5$, provided the closest agreement with the measured $X(t)$ trends across the datasets.

From the analysis, the crystallisation progress was then fitted using the reduced Avrami-type form when $n = 0.5$:

$$X(t) = 100 \times \left(1 - e^{-kt^{0.5}}\right) \tag{4}$$

In Eq. (4), the exponent must be dimensionless; therefore *k* has units of $min^{-0.5}$. The parameter *k* was estimated by least-squares regression of Eq. (2) against the experimental $X(t)$ values. Worth noting that, in this analysis, the parameter *k* governs the time scale of the crystallisation progress curve of which, higher *k* indicates faster crystallisation under the same experimental and image-processing condition.

To report the pointwise mismatch between the measured data and the fitted curve (as a fit residual rather than experimental uncertainty), the absolute residual at each time point was calculated as:

$$Absolute\ difference = \left|X_{data} - X_{fit}\right| \tag{5}$$

where X_{data} is the image-derived crystallised fraction and X_{fit} is the fitted value from Eq. (2).

Because n was fixed at 0.5, k has units of $min^{-0.5}$ in Eq. (4). For interpretability, a characteristic half-crystallisation time $t_{50} = \left(\frac{ln\,2}{k}\right)^2$ was also reported in which lower t_{50} indicates faster crystallisation. From Eq. (2), set $X(t) = 50$:

$$50 = 100\left(1 - e^{-kt_{50}^{0.5}}\right) \tag{6}$$

$$\text{Which gives, } e^{-kt_{50}^{0.5}} = 0.5 \text{ which then solved to } t_{50} = \left(\frac{ln\,2}{k}\right)^2 \tag{7}$$

3. RESULTS AND DISCUSSION

3.1. TEMPERATURE AND CUMULATIVE ENTHALPY ANALYSIS

The temperature and cumulative enthalpy analysis have been discussed in detail by the current researchers in (Jarimi et al. 2026). Noting that, during the melting experiments, all samples were exposed to a temperature of 140 °C to facilitate a comprehensive thermal transition. The analytical focus on phase change materials (PCMs) will concentrate on the temperature profile characterizing the melting phase of sugar alcohols. Figure 7a depicts the melting curve of erythritol, which distinctly demonstrates the characteristics of a mono PCM. Initially, there was a rapid increase in temperature to approximately 118 °C, followed by a noticeable quasi-plateau where the temperature increment significantly decelerates. This narrow plateau, cantered around 118 °C, indicates the high purity and well-defined phase change properties of erythritol. Upon completion of melting, the temperature continues to ascend beyond 120 °C due to the heat source, signifying the sensible heating of the liquid phase. Similarly, as illustrated in Figure 7b, xylitol exhibits a moderately defined quasi-plateau between 90 °C and 100 °C, consistent with its melting point as documented in the literature. In this study, the melting slope is more gradual, indicating a distributed melting process. Subsequent to the phase transition, the temperature continues to rise, indicating the sensible heating of the completely melted PCM. Figure 8a reveals that the binary non-eutectic mixture of xylitol and erythritol exhibits an even more diffuse melting behaviour. A weak quasi-plateau is observed from 90 °C to 110 °C, lacking a clearly defined inflection point. This suggests incongruent melting, where the individual components undergo phase changes at different temperatures rather than simultaneously. Consequently, there was a spread-out latent heat absorption, diminishing the sharp thermal response typically desired in thermal energy storage. Subsequently, a more pronounced temperature increases beyond 110 °C indicates that the melting process was largely complete, transitioning to the sensible heating region. The binary eutectic mixture illustrated in Figure 8b presents a more synchronized and defined quasi-plateau compared to its non-eutectic counterpart. Following the initial sensible heating phase from approximately 50 °C to about 90 °C, the temperature curve exhibits a moderate flattening between 90 °C and 120 °C. This indicates co-melting behaviour at a specific eutectic composition, where both components transition concurrently. Although the plateau was not perfectly flat, its relative clarity and narrower span suggest improved thermal uniformity and predictability.

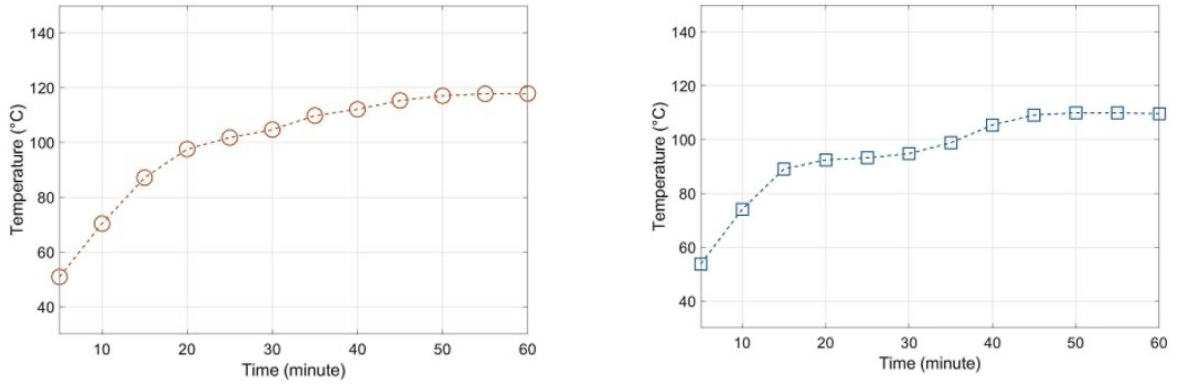

(**a**) (**b**)

Figure 7. The melting profile for the **(a)** Erythritol and **(b)** Xylitol (Jarimi et al. 2026).

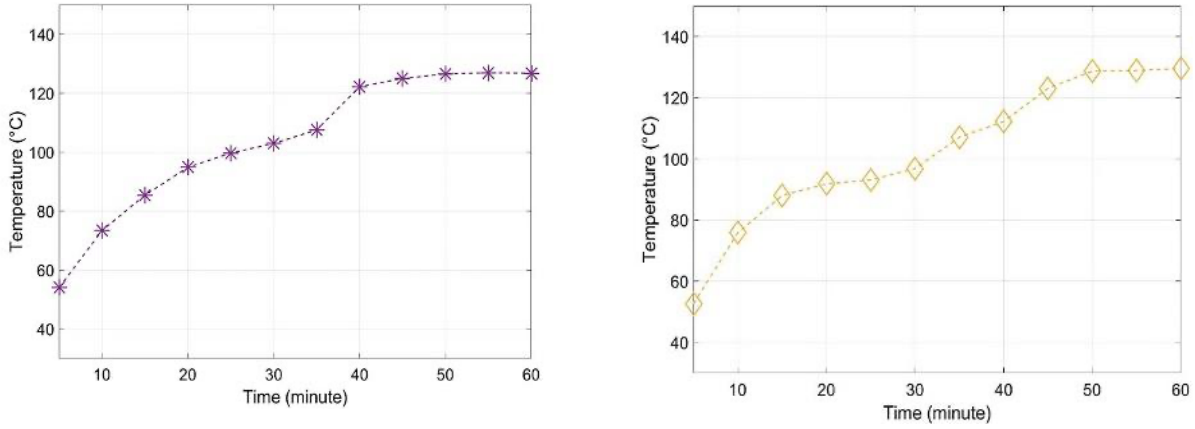

(**a**) (**b**)

Figure 8. **(a)** The melting profile for binary non-eutectic mixture of xylitol and erythritol and **(b)** binary eutectic mixture of xylitol and erythritol (Jarimi et al. 2026).

In a related context, the phenomena of supercooling and unintended crystallization of the samples were assessed utilizing both sensible cooling methodologies and visual inspection techniques. As depicted in Figure 9(a), during the cooling process, a rapid escalation in temperature from approximately 70 °C to approximately 118 °C occurs, signifying the abrupt crystallization of Erythritol due to its degree of supercooling. Conversely, other samples demonstrated a similar temperature decline over time, as illustrated in Figure 9(b), indicating the supercooling characteristic of these materials. Despite the temperature descending significantly below the melting point, these materials remained in a stable metastable state (liquid state) and exhibited no crystallization phenomena. Nevertheless, due to constraints inherent in the experimental setup, this study implemented cold crystallization heating immediately upon the samples achieving ambient temperature stability. This approach does not affect cumulative enthalpy calculations, as performance is independent of time.

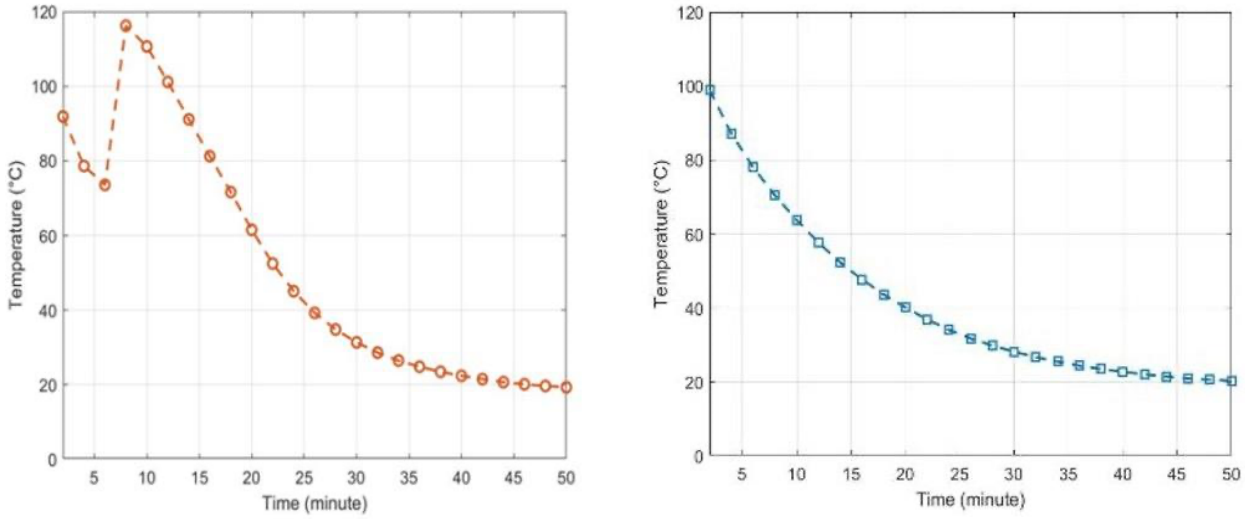

(**a**) (**b**)

Figure 9. **(a)** Supercooling profile for Erythritol and **(b)** xylitol. Please note that other samples show a similar trend to Xylitol with unobservable visual differences on the graph (Jarimi et al. 2026).

In this study, Figure 10 represents the cumulative enthalpy against temperature of the PCM which is defined such that the enthalpy is set to zero at the onset of crystallization. This approach isolates the exothermic energy released during crystallization and allows direct comparison of the latent heat released by different samples. For erythritol, repeated tests showed poor controllability; however, the maximum temperature reached during crystallization was approximately 116.44 °C when crystallization occurred after starting to crystallise at 70 °C. The average cumulative enthalpy computed was about 358.38 kJ/kg.

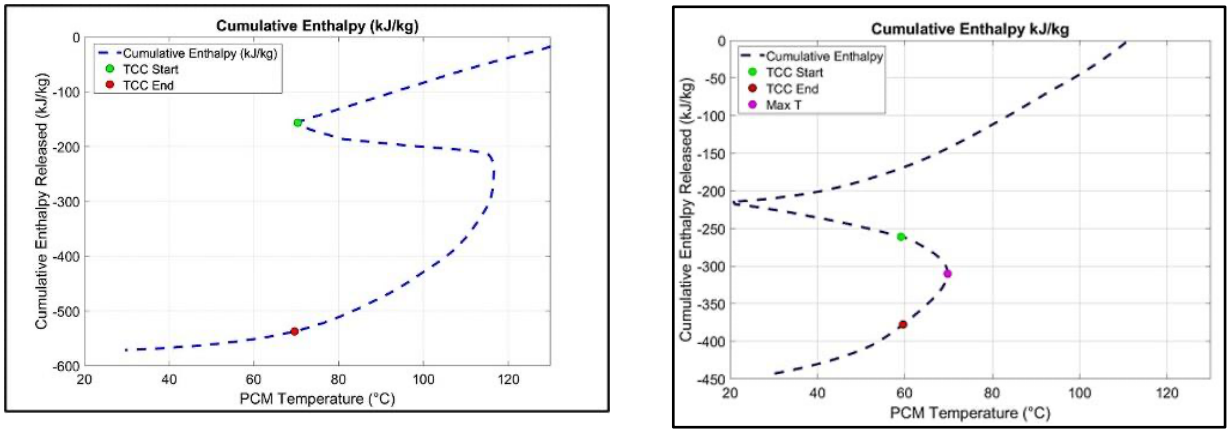

(**a**) (**b**)

Figure 10. The cumulative enthalpy against temperature for binary supercooled PCMs for **(a)** Erythritol and **(b)** Xylitol (Jarimi et al. 2026).

For xylitol and the binary mixtures (Xy-Er) eut and non-eutectic (Xy-Er), crystallization did not occur unintentionally during cooling and was initiated by applying a temporary heat input up to 60 °C. This can be clearly seen from the trend of cumulative enthalpy curve in way that the temperature curve dropped to 20 ºC before re-heated to initiate crystallisation. But for erythritol, the temperature drops only until 70 ºC. As illustrated in Figure 11, under these conditions, the cumulative enthalpy released by xylitol was approximately 116.53 kJ/kg. For the eutectic mixture (Xy-Er)eut, the cumulative enthalpy was 133.89 kJ/kg, while the non-eutectic binary (Xy-Er) sample exhibited a higher cumulative enthalpy of 287.78 kJ/kg. These results indicate that the non-eutectic binary (Xy-Er) mixture provides more effective latent heat release under the applied triggering conditions and was therefore selected for the subsequent detail triggering analysis.

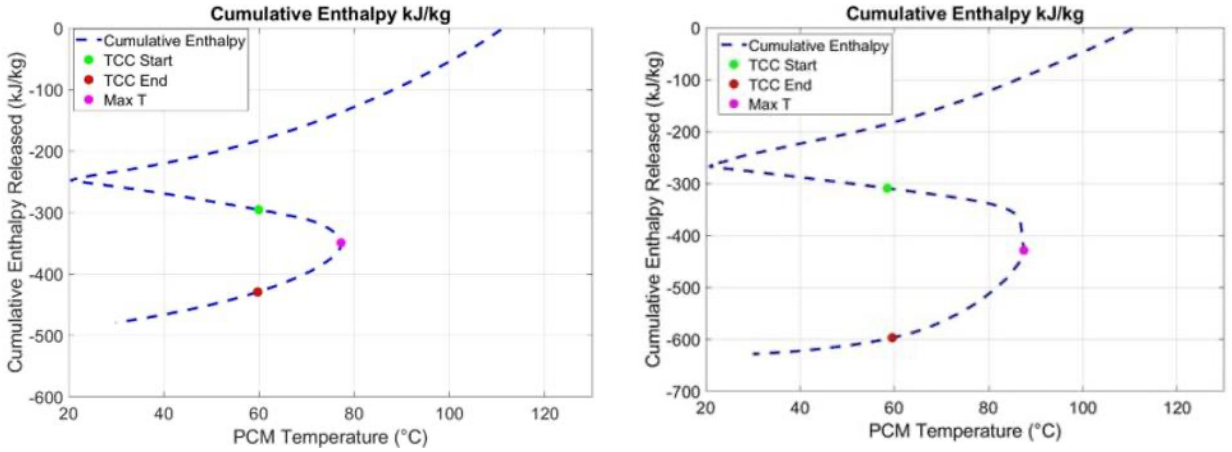

(**a**) (**b**)

Figure 11. The cumulative enthalpy against temperature for binary supercooled PCMs for **(a)** non-eutectic binary (Xy-Er) mixture and **(b)** eutectic binary (Xy-Er) (Jarimi et al. 2026).

Table 3 presents the calculated cumulative enthalpy values obtained from the onset of cold crystallisation at 60 °C and back, along with the corresponding crystallisation peak temperatures of the samples and their associated errors. Based on the data in Table 3, the non-eutectic erythritol–xylitol (Xy–Er) mixture tested under the high heating-rate condition was chosen for further analysis, as it exhibits a higher crystallisation peak temperature while still maintaining a high cumulative enthalpy during cold crystallisation.

Table 3. The summary of the comparison between the samples. The binary non-eutectic sample has been selected for the simulation case study (Jarimi et al. 2026).

Materials	**Cold-crystallisation heat or enthalpy ΔH_{cc} (kJ/kg)**	**Peak temperature $T_{cc,peak}$ (˚C)**
Erythritol	358.38±5.65	116.00±1.1
Xylitol (Heating rate 1)	16.21± 5.53	59.68 ±1.1
Xylitol (Heating rate 2)	116.53 ±13.24	69.77±1.1
(Xy-Ery)eut (Heating rate 1)	133.89±13.09	77.23 ±1.1
(Xy-Ery)eut (Heating rate 2)	84.84±12.43	61.65 ±1.1
Xy-Ery (Heating rate 1)	177.93 ±16.09	73.26 ±1.1
Xy-Ery (Heating rate 2)	287.78±17.18	87.47 ±1.1

3.2. CRYSTALLISATION OBSERVATION

The crystallisation behaviour of the non-eutectic binary xylitol–erythritol (Xy–Er) mixture was analysed using an observational imaging method. Crystallisation progress was monitored from 1 to 40 min after triggering. This duration was selected based on preliminary trials indicating that the most significant stages of nucleation and early growth occur within the first 40 min. Crystallisation progress was quantified from processed images as the crystallised area fraction, and the resulting progress curves were analysed over the 5–40 min interval. Noting that, the crystallisation behaviour was observed with the testing repeated at average of 3 times with only the most consistent observation was selected. The average temperature of the surrounding was maintained under a controlled environment at ± 1.1 °C.

To enable direct comparison across triggering approaches, all image-derived crystallisation progress curves were fitted using a reduced Avrami-type model with fixed exponent $n = 0.5$. This with the derived characteristic half-crystallisation time of $t_{50} = \left(\frac{ln2}{k}\right)^2$ in Equation (6) have been beinterpreted as comparative metrics under identical experimental and image-processing conditions. Two thermal conditions were investigated throughout: case A (30 °C) and case B (60 °C following the cold-crystallisation condition).

3.2.1. SEEDING

Figures 12 and 13 present the crystallization behaviour of the selected supercooled phase change materials (PCMs), induced by a crystallization seed, under two thermal conditions: cooling to 30 °C and pre-heating to 60 °C, hereafter referred to as case A and case B, respectively. Comparative analysis reveals that the elevated viscosity and reduced internal energy of the PCMs when triggered in case A, led to a markedly slower crystallization process. After 40 minutes, the samples that were triggered in case B which was subjected to cold crystallisation with seeding pre reached approximately 75% crystallization after 40 minutes of triggering, whereas the sample which was maintained at 30 °C in case A attained only about 30% crystallization. These observations indicate that seeding alone, without the application of cold crystallization, is not an effective approach, primarily due to the high viscosity of the supercooled material, which substantially impedes crystallization (Aladool, Aziz & Wright 2017). In addition, this observation may also be attributed by the increased viscosity which diminishes molecular mobility and mass transfer rates, thereby restricting diffusion and hindering the orderly molecular rearrangement required for crystal lattice formation.

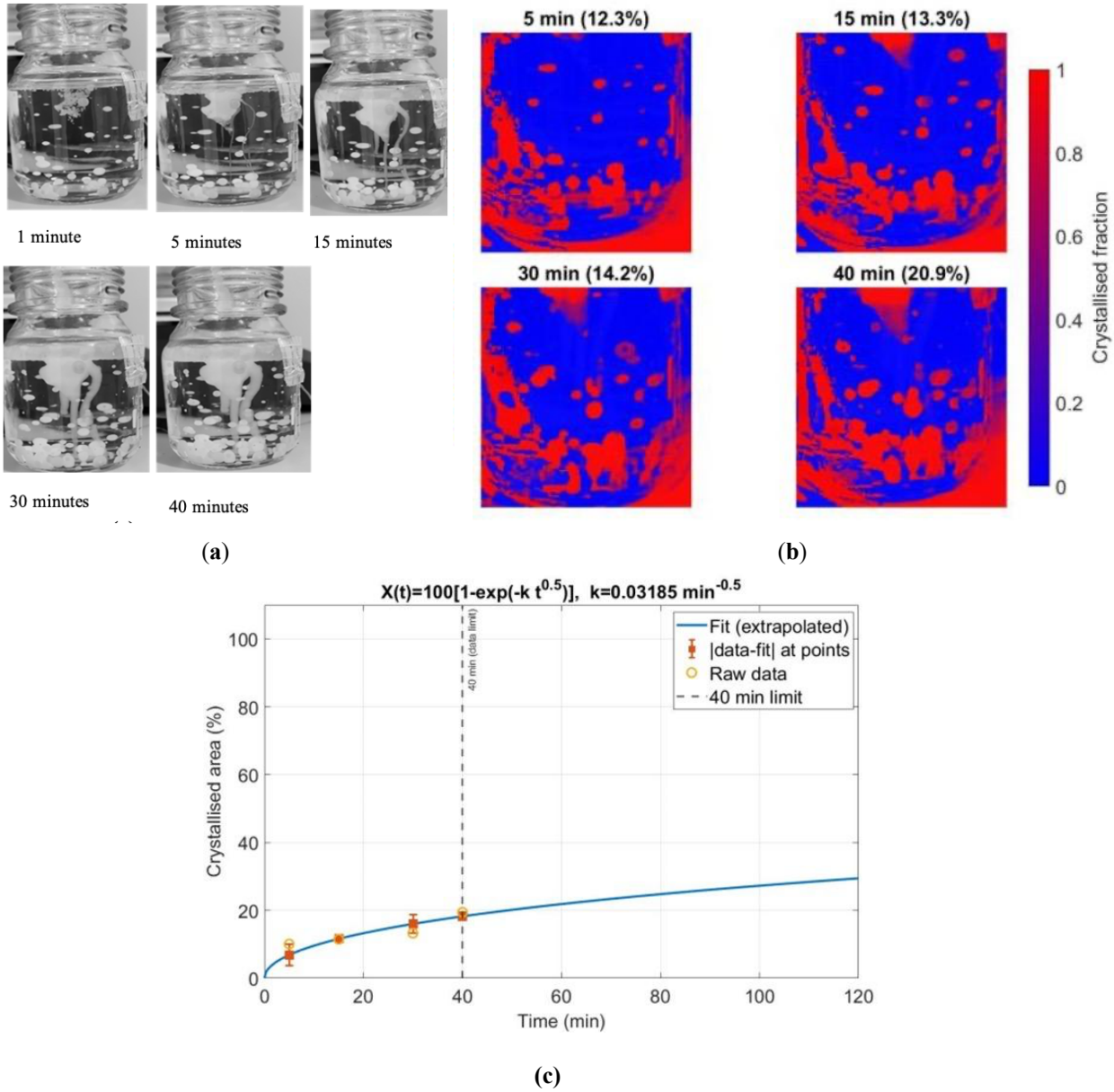

Figure 12. **(a)** Captured images of the supercooled PCM during crystallisation following seeding under case A (30 °C) at 5–40 min. **(b)** Processed crystallisation maps (colour scale: crystallised fraction 0–1) and **(c)** kinetic fit using the reduced Avrami-type model with fixed exponent $n = 0.5$. Error bars show the absolute difference between the measured crystallised area fraction and the fitted value at each time point.

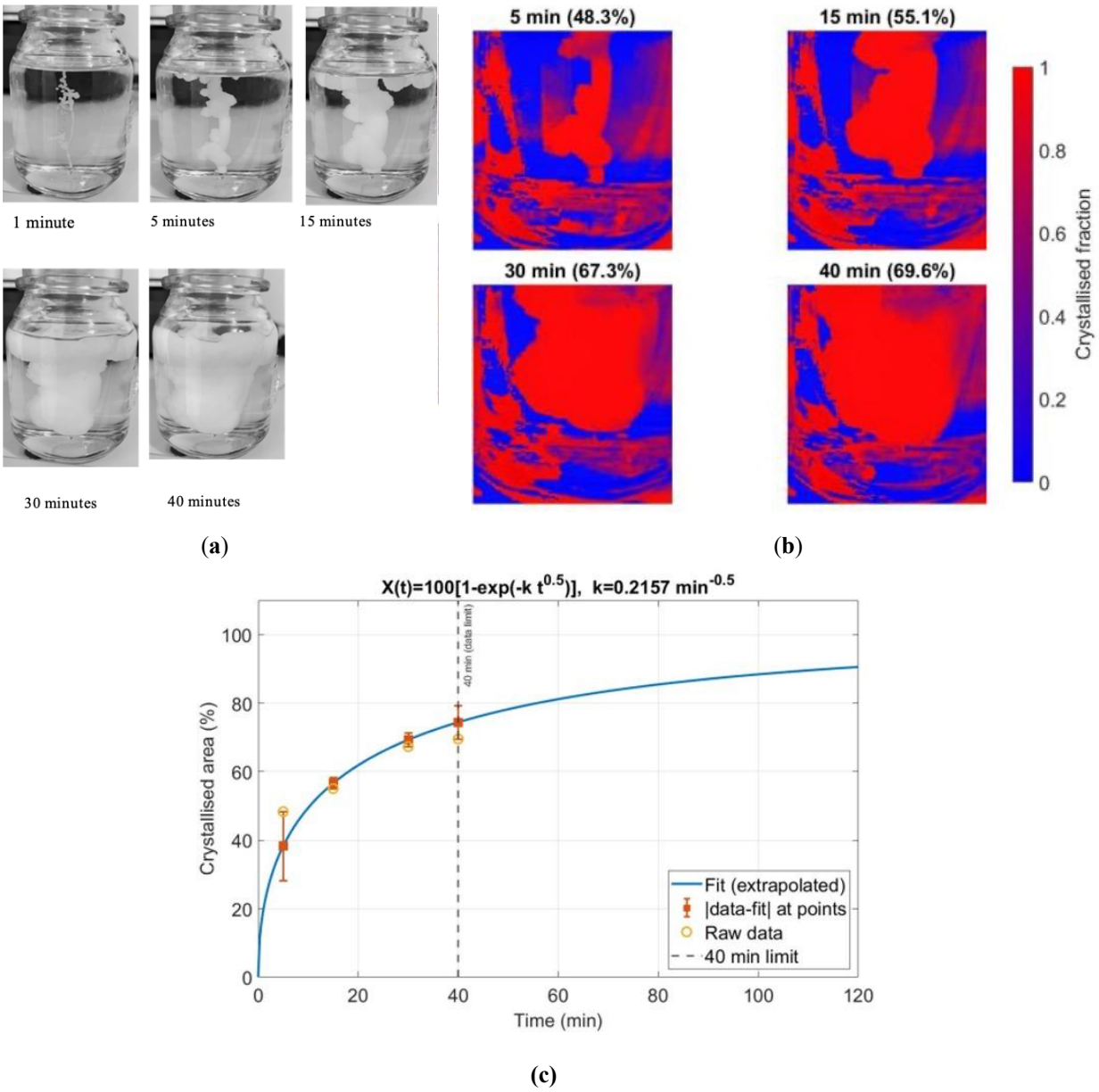

Figure 13. **(a)** Captured images of the supercooled PCM during crystallisation following seeding under case B (60 °C) after the cold-crystallisation condition at 5–40 min. **(b)** Processed crystallisation maps (colour scale: crystallised fraction 0–1) and **(c)** kinetic fit using the reduced Avrami-type model with fixed exponent n = 0.5. Error bars show the absolute difference between the measured crystallised area fraction and the fitted value at each time point.

Image-processing-based analysis further shows that the Avrami-type progress model provides a satisfactory representation of crystallisation under both thermal conditions. For the case B, the absolute residuals were 3.20 %, 0.10 %, 2.72 % and 1.20 % at 5, 15, 30 and 40 min, respectively, indicating close agreement after the earliest time point. For case B, residuals remained within 1.56–10.07 % over 5–40 min, with the maximum deviation at 5 min, suggesting that a significant portion of crystallisation occurred rapidly immediately after seeding and was not fully resolved by the discrete imaging times. These trends are consistent with viscosity-controlled behaviour: under case A, higher viscosity reduces molecular mobility and diffusion, slowing growth from the seed, whereas under case B reduced viscosity enhances transport and promotes faster crystallisation propagation.

Consistent with these observations, the fitted kinetic parameter for the case B is $k = 0.2157\ min^{-0.5}$ (RMSE = 5.74 %), corresponding to a rapid increase in crystallised fraction from 48.3 % (5 min) to 69.6% (40 min). In contrast, the case A dataset yielded a much smaller kinetic parameter, $k = 0.03185\ min^{-0.5}$ (RMSE

= 2.18 %), consistent with the lower crystallised fraction of 10.1–19.4 % between 5 and 40 min. Overall, pre-heating to 60 °C in case B increased the apparent crystallisation kinetics by a factor of approximately 6.8 relative to 30 °C, in agreement with the substantially larger crystallised fraction observed in Figure 13 compared with Figure 12 over the same 40 min interval. Meanwhile, using the characteristic half-crystallisation time t_{50}, seeding corresponds to $t_{50}\approx$ 474min (≈ 7.9 h) in case A but only $t_{50}\approx$ 10.3min in case B, confirming a strong acceleration when the PCM was pre-heated to 60 °C.

3.2.2. TEC HEAT SINK

Figure 14 shows the crystallisation response of the supercooled PCM to a localised cooling shock introduced using a thermoelectric cooler (TEC) under case B (60 °C). The image-derived crystallised area fraction increased only marginally from 5.3% (5 min) to 9.8% (15 min) and then progressed slowly to 10.3% (30 min) and 13.2% (40 min). The crystallisation maps indicate that transformed regions remained spatially localised and did not propagate substantially through the bulk during the observation window, demonstrating that the TEC-induced perturbation did not create a sufficiently strong or sustained nucleation-and-growth process.

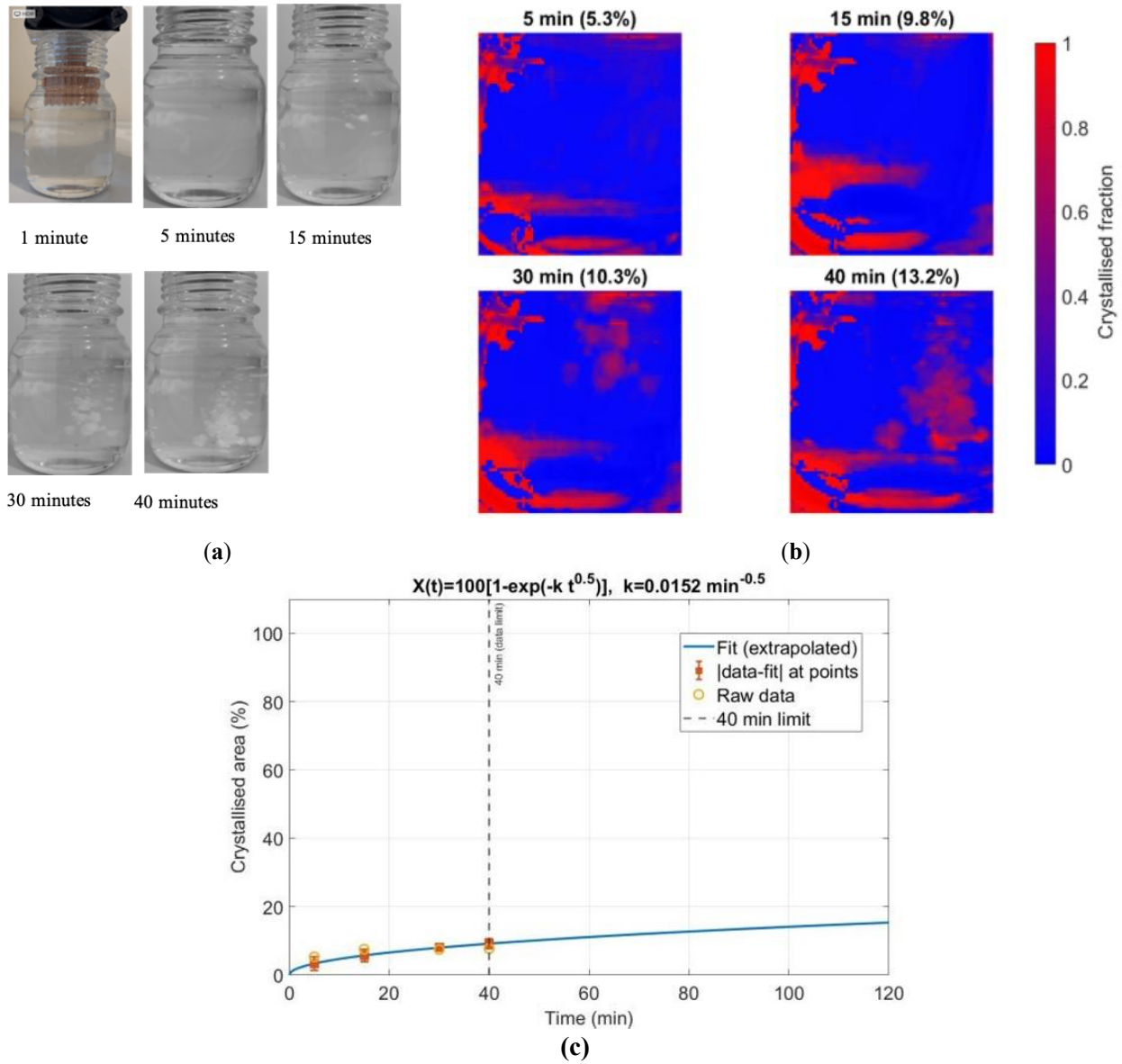

Figure 14. **(a)** Captured Images of the supercooled PCMs through observation from 1 to 40 minutes during crystallisation after introducing a cold shock at a PCM temperature of 60 °C (case B). **(b)** Processed crystallisation maps (colour scale: crystallised fraction 0–1) and **(c)** kinetic fit using the reduced Avrami-type model with fixed exponent n = 0.5.

This weak response is consistent with practical limitations of the current TEC implementation. Commercial

TEC modules are typically planar and square, which constrains the achievable cooling intensity at a local "tip" and limits the formation of steep temperature gradients within the PCM. In addition, the effective cooling at the contact point can be reduced by thermal contact resistance, lateral heat spreading through the heat sink, and rapid heat replenishment from the warm bulk PCM. Consequently, the local undercooling may remain below the threshold required to reliably initiate heterogeneous nucleation. Even if transient nuclei form near the cooled region, growth may be impeded by insufficient driving force and by the balance between local cooling and heat inflow from the surrounding PCM.

Consistent with the visual and map-based observations, the reduced Avrami-type fit with fixed exponent n = 0.5 yielded a small kinetic parameter, $k = 0.0152\, min^{-0.5}$. Using Eq. (2), the fitted curve predicts crystallised fractions of approximately 3.34%, 5.72%, 7.99% and 9.17% at 5, 15, 30 and 40 min, respectively. The corresponding absolute residuals (measured – fitted) are therefore 1.96%, 4.08%, 2.31% and 4.03%, indicating that the model captures the slow-progress trend but underestimates the measured fractions, likely due to early localised crystallisation and segmentation artefacts that are not fully resolved by discrete imaging times. A characteristic half-crystallisation time derived from the fitted parameter, $t_{50} = \left(\frac{ln\,2}{k}\right)^2$, is approximately 2079 min (~34.6 h), reinforcing that TEC triggering is extremely slow and ineffective for rapid, on-demand crystallisation with the present setup.

3.2.3. ELECTRIFICATION

Figures 15 and 16 present crystallisation initiated by electrification (4.5 V applied for 1 min) under case A (30 °C) and case B (60 °C, following cold-crystallisation condition). A strong thermal dependence is evident. Under case A, crystallisation remains limited and appears to plateau within the 40 min observation window. The image-derived crystallised area fraction increases only modestly from 5.9% (5 min) to 7.8% (15 min), reaching 9.0% (30 min) and remaining at 9.0% (40 min). The processed crystallisation maps show nucleation primarily localised around the electrode region with little subsequent propagation into the bulk, indicating that although the applied potential can initiate local nuclei, bulk growth remains strongly hindered.

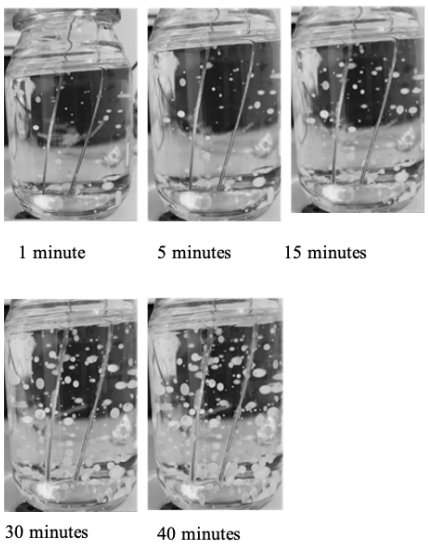

(**a**)

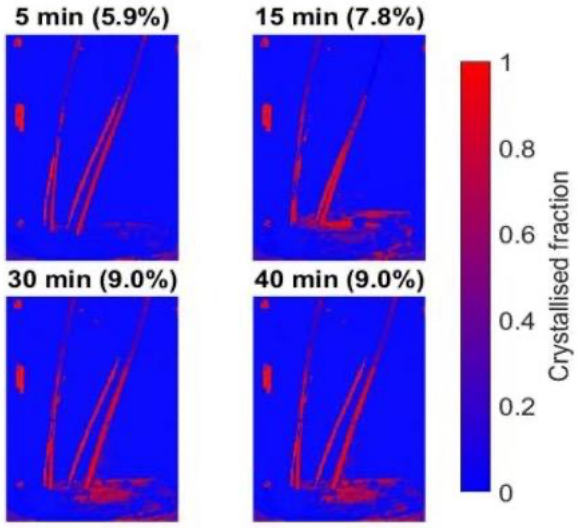

(**b**)

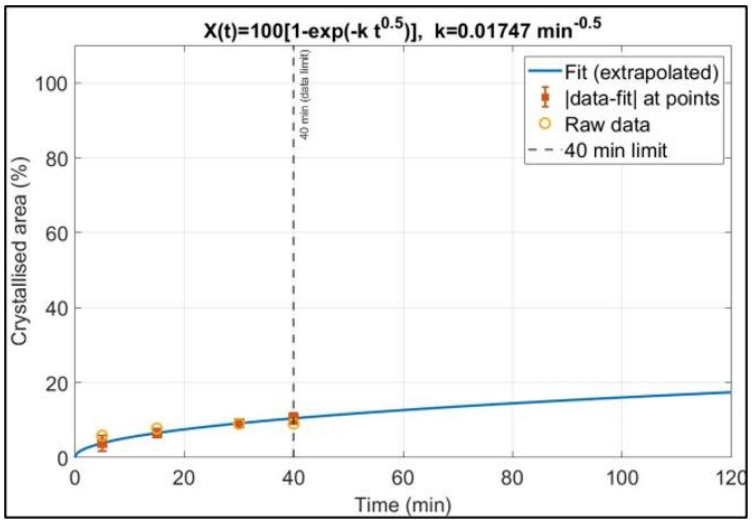

(**c**)

Figure 15. **(a)** Captured images of the supercooled PCM during crystallisation following electrification (4.5 V applied for 1 min) at a PCM temperature of 30 °C (case A). **(b)** Processed images showing crystallisation maps (colour scale: crystallised fraction 0–1). **(c)** Kinetic fit using the reduced Avrami-type model with fixed exponent n = 0.5. Error bars show the absolute difference between the measured crystallised area fraction and the fitted value at each time point.

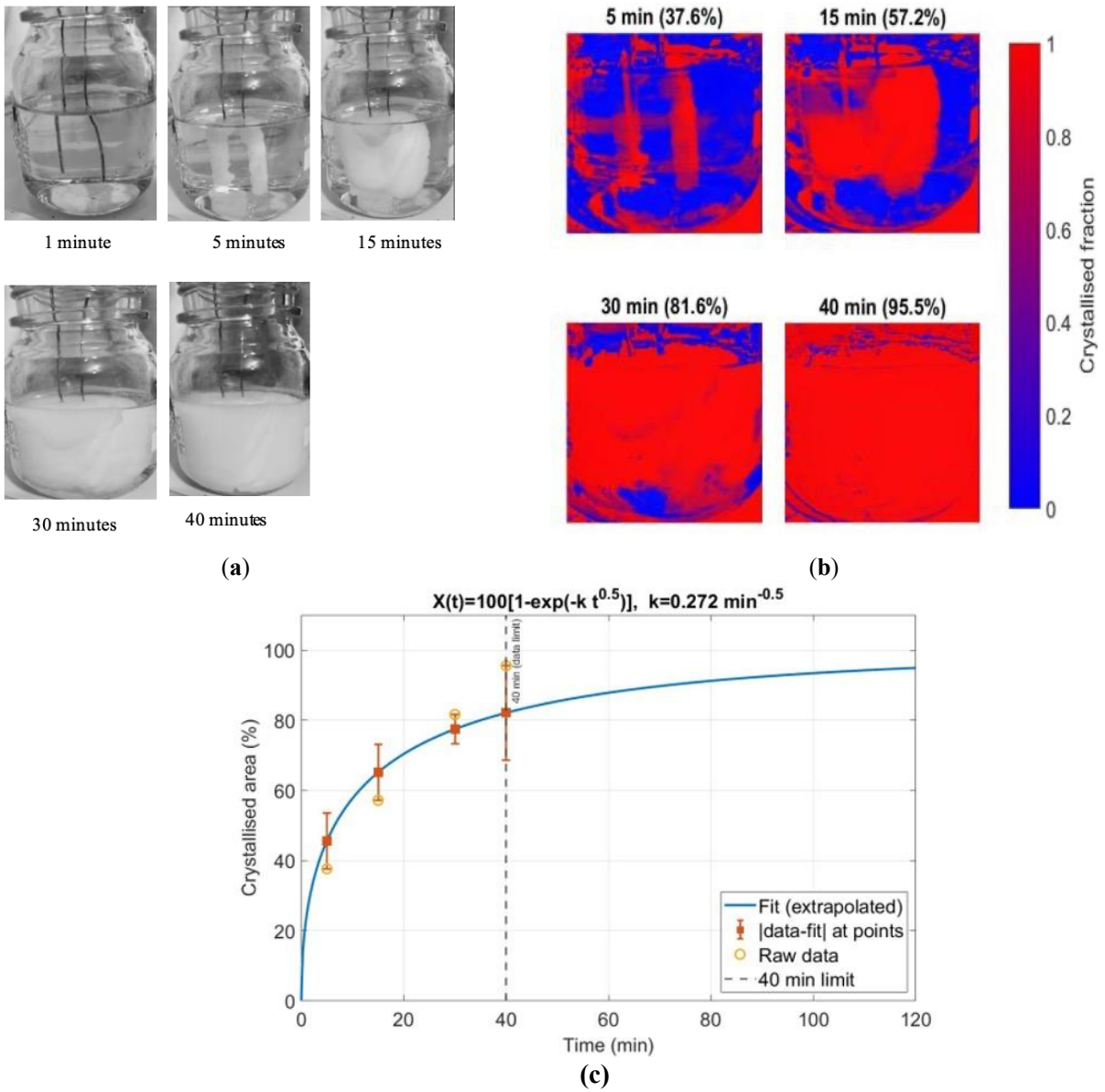

Figure 16. **(a)** Captured images of the supercooled PCM during crystallisation following electrification (4.5 V applied for 1 min) at a PCM temperature of 60 °C (case B) after the cold-crystallisation condition. **(b)** Processed crystallisation maps (colour scale: crystallised fraction 0–1). **(c)** Kinetic fit using the reduced Avrami-type model with fixed exponent n = 0.5. Error bars show the absolute difference between measured and fitted crystallised area fraction at each time point.

In contrast, electrification under case B produces rapid and extensive crystallisation throughout the sample volume. The crystallised area fraction increases from 37.6% (5 min) to 57.2% (15 min), reaching 81.6% (30 min) and 95.5% (40 min). The crystallisation maps confirm fast propagation and coalescence of crystallised regions, culminating in near-complete conversion by the end of the measurement period. This behaviour is consistent with viscosity-controlled kinetics of which at the lower temperature in case A, elevated viscosity suppresses molecular mobility and diffusion-limited growth, whereas at the higher temperature in case B, reduced viscosity supports both growth and the spread of crystallisation once nucleation was initiated. In addition, electrification may promote heterogeneous nucleation at the electrode surface and in its vicinity (e.g., through interfacial effects and local field-induced perturbations), but the extent to which this leads to bulk conversion is ultimately governed by transport and growth conditions.

Image-processing-based analysis shows that the reduced Avrami-type progress model with fixed exponent n = 0.5 provides a reasonable comparative description of the electrification datasets. Using Eq. (2) with $k = 0.01747\ min^{-0.5}$, the fitted values are approximately 3.83%, 6.54%, 9.13% and 10.46% at 5, 15, 30 and 40 min, giving absolute residuals of 2.07%, 1.26%, 0.13% and 1.46%, respectively (case A). For case B ($k = 0.272\ min^{-0.5}$), the fitted values are approximately 45.57%, 65.13%, 77.46% and 82.10%, giving

absolute residuals of 7.97%, 7.93%, 4.14% and 13.40%, respectively. The larger deviations in case B are consistent with the observed rapid conversion (especially at later times) and indicate that a single fixed exponent (n = 0.5) may under-represent the accelerating, bulk-propagating behaviour under electrification at elevated temperature. Nevertheless, the fitted kinetic parameters clearly capture the strong enhancement between the two conditions: kincreases from 0.01747 to 0.272 $min^{-0.5}$ (approximately 15.6 higher), consistent with the transition from weak, localised crystallisation in case A to near-complete conversion in case B.

In addition, based on the reduced Avrami-type fit (n = 0.5), the characteristic half-crystallisation time t_50 computed using Eq. (5) was 1574 min (26.2 h) for electrification in case A ($k = 0.01747\ min^{-0.5}$), but only 6.49 min in case B ($k = 0.272\ min^{-0.5}$), confirming a strong temperature-dependent acceleration for this triggering method.

3.2.4. MECHANICAL AGITATION

Figures 17 and 18 show crystallisation initiated by mechanical agitation under case A (30 °C) and case B (60 °C, following the cold-crystallisation condition). Mechanical agitation produced the most rapid and spatially widespread crystallisation among the triggering strategies examined, with high crystallised fractions achieved even under case A. Under case A, the image-derived crystallised area fraction increased from 49.4% (5 min) to 59.9% (15 min) and 61.8% (30 min), reaching 72.8% (40 min). The crystallisation maps indicate that agitation generates distributed nucleation sites throughout the sample volume rather than relying on localised initiation, enabling comparatively rapid bulk conversion despite the higher viscosity at 30 °C.

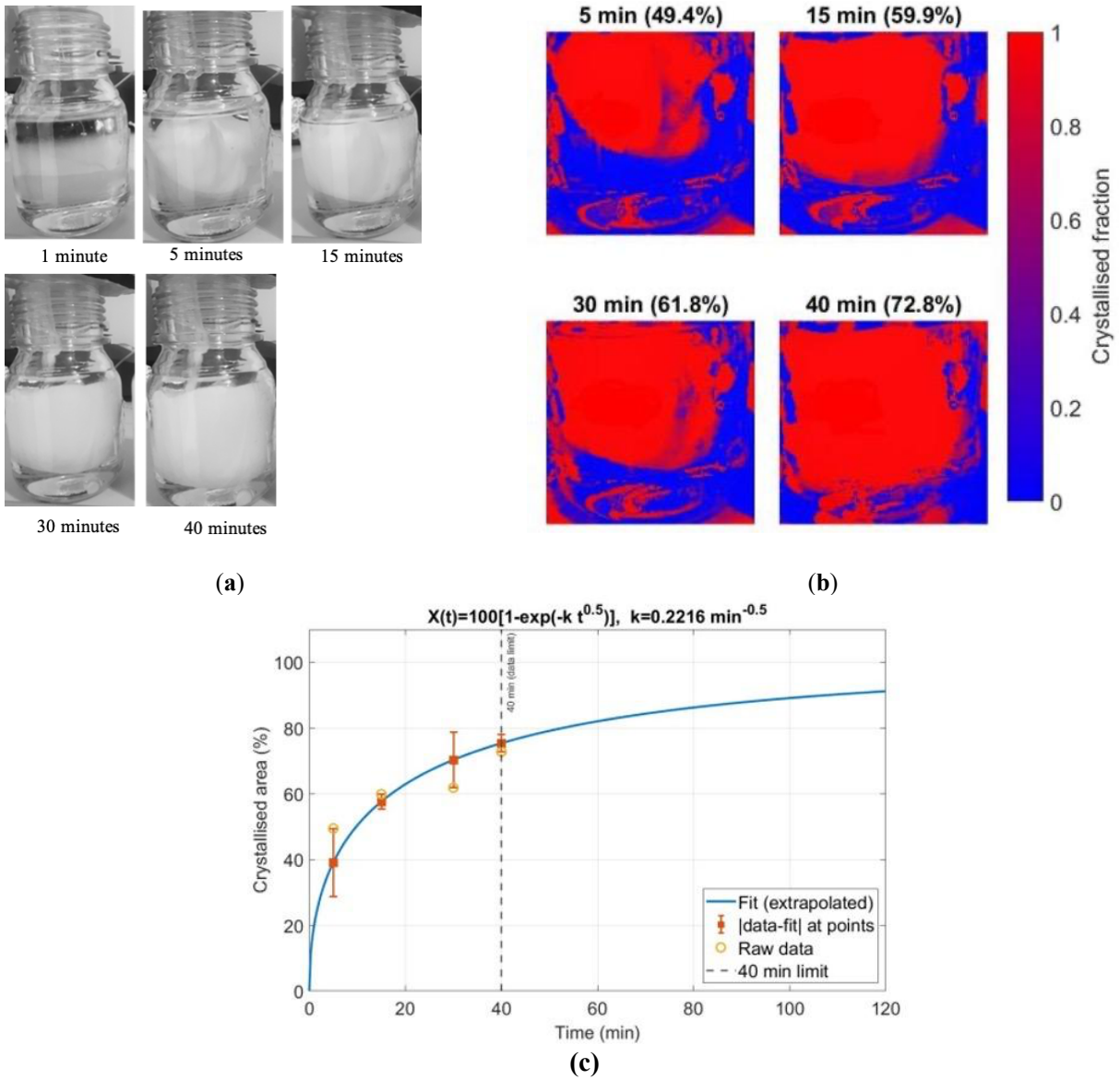

Figure 17. **(a)** Captured images of the supercooled PCM during crystallisation following mechanical agitation at 30 °C (case A). **(b)** Processed crystallisation maps (colour scale: crystallised fraction 0–1) and **(c)** kinetic fit using the reduced Avrami-type model with fixed exponent n = 0.5. Error bars show the absolute difference between the measured crystallised area fraction and the fitted value at each time point.

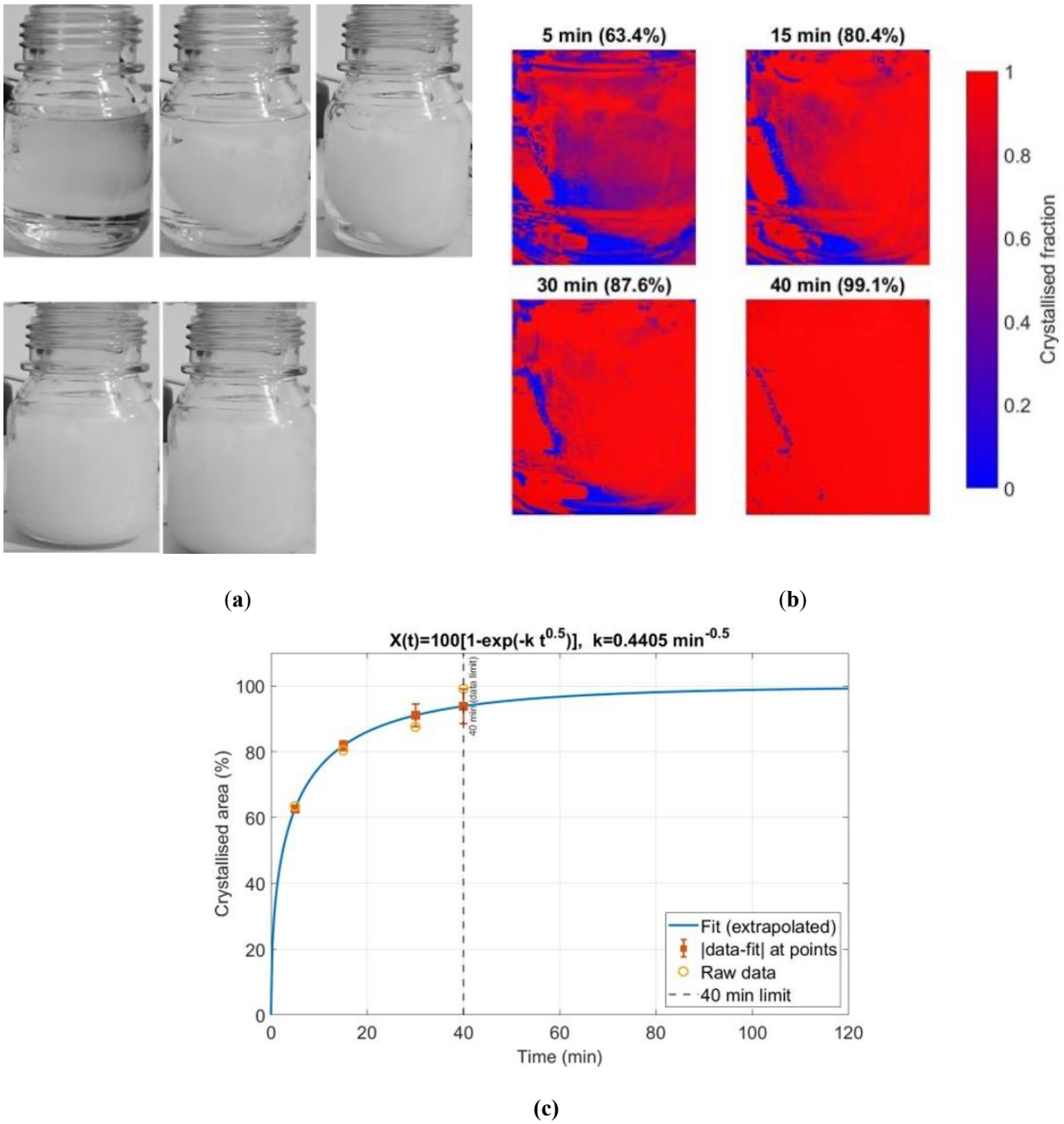

Figure 18. **(a)** Captured images of the supercooled PCM during crystallisation following mechanical agitation at 60 °C (case B) after the cold-crystallisation condition. **(b)** Processed crystallisation maps (colour scale: crystallised fraction 0–1) and **(c)** kinetic fit using the reduced Avrami-type model with fixed exponent n = 0.5. Error bars show the absolute difference between measured and fitted crystallised area fraction at each time point.

Under case B, agitation further accelerated crystallisation and produced near-complete conversion within the 40 min window. The crystallised area fraction rose from 63.4% (5 min) to 80.4% (15 min) and 87.6% (30 min), reaching 99.1% (40 min). The processed maps show extensive propagation and coalescence of crystallised regions, consistent with reduced viscosity at elevated temperature supporting faster growth and more effective heat/mass transport during crystallisation.

The reduced Avrami-type progress model with fixed exponent n = 0.5 was fitted to both datasets to enable direct comparison across triggering methods. For case A, the fitted parameter was $k = 0.2216\ min^{-0.5}$, giving fitted values of approximately 39.04%, 52.52%, 65.41% and 71.19% at 5, 15, 30 and 40 min, respectively. The corresponding absolute residuals are 10.36%, 7.38%, 3.61% and 1.61%, showing that deviations are largest at the earliest time point, likely reflecting very rapid crystallisation immediately after stirring that was not fully resolved by the discrete observation times. For case B, $k = 0.4405\ min^{-0.5}$yields fitted values of approximately 62.69%, 81.85%, 91.20% and 93.81%, with absolute residuals of 0.71%, 1.45%, 3.60% and

5.29%. Overall, the fit captures the fast, saturating behaviour well, with slightly increased mismatch at later times as conversion approaches completion.

A characteristic half-crystallisation time derived from the fitted kinetics, $t_{50} = \left(\frac{ln\,2}{k}\right)^2$ from Eq. (5) further highlights the effectiveness of agitation. Under case A, $t_{50} \approx 9.79$ min, indicating rapid crystallisation even without pre-heating. Under case B, $t_{50} \approx 2.47$ min, confirming that agitation combined with the elevated-temperature condition provides the fastest overall conversion. From kinetics point of view, agitation is expected to enhance crystallisation by disrupting the metastable supercooled structure, increasing collision frequency and molecular rearrangement, and inducing secondary nucleation via shear, thereby reducing the nucleation barrier and enabling rapid growth throughout the bulk volume. These results demonstrate that mechanical agitation is the most promising method for achieving reliable, high-fraction crystallisation of the selected supercooled sugar-alcohol PCM within short time windows.

Table 4. The summary of the triggering method and its kinetic crystallisation observation.

Triggering method	**k ($min^{-0.5}$) Case A**	**t_{50} (min) Case A**	**k ($min^{-0.5}$) Case B**	**t_{50} (min) Case B**	**Relative change (B/A)**	**Key observation**
Seeding	0.03185	474	0.2157	10.3	6.77	Crystallised fraction rose from ~30% (30 °C) to ~75% (60 °C) at 40 min
TEC localised cooling	Not tested	—	0.0152	2079	—	Insignificant crystallised area changes over 40 min
Electrode triggering	0.01747	1574	0.272	6.49	15.57	<10% crystallised in case A strong acceleration in case B with applied potential
Mechanical agitation	0.2216	9.79	0.4405	2.47	1.99	Strongest overall enhancement; highest apparent crystallisation rates

*Note: Case A = 30 °C; case B = 60 °C following the cold-crystallisation condition. $t_{50} = \left(\frac{ln\,2}{k}\right)^2$. TEC was not tested in case A.

4. CONCLUSION

This study investigated several triggering mechanisms for controlling crystallisation in supercooled sugar-alcohol PCMs, including seeding, TEC heat sink (localised cooling), electrode-based triggering, mechanical agitation, and thermal conditioning via cold crystallisation. It should be noted that the crystallisation kinetics reported here do not represent intrinsic material properties but are used for comparative purposes. The work began with screening binary and ternary sugar-alcohol mixtures to identify candidates operating in the 50–80 °C range with sufficiently high latent heat and supercooling stability. Based on the experimental observations and kinetic analysis, the following conclusions can be drawn:

1. Erythritol exhibited the highest cumulative enthalpy (358.66 kJ/kg), but showed poor controllability due to unintentional premature crystallisation, limiting its suitability for controllable supercooling applications.
2. Xylitol and xylitol–erythritol (Xy–Er) mixtures demonstrated stronger supercooling stability, indicating better potential for on-demand heat release when appropriate triggering is applied.
3. Under triggered conditions, the non-eutectic Xy–Er mixture released approximately 287.78 kJ/kg, providing the best balance between substantial latent heat delivery and controllable supercooling. Although this is lower than erythritol, it offers improved controllability.
4. The eutectic Xy–Er mixture and pure xylitol produced lower released energies (133.89 kJ/kg and 116.53 kJ/kg, respectively), confirming that the non-eutectic mixture was the most effective among the controllable supercooled samples tested.
5. Crystallisation behaviour in the selected non-eutectic Xy–Er mixture was strongly influenced by both triggering strategy and thermal condition, confirming that thermal conditioning is critical for rapid and reliable discharge.
6. Seeding showed strong temperature dependence: the measured crystallised area fraction at 40 min increased from 20.9 % (30 °C, case A) to 69.6% (60 °C, case B). Consistently, the fitted kinetics increased

from $k = 0.03185$ to $0.2157\ min^{-0.5}$, corresponding to a reduction in characteristic half-crystallisation time from $t_{50} \approx 474$min to $t_{50} \approx 10.3$min, indicating that seeding alone is ineffective at 30 °C within the 40-min window.

7. TEC-based localised cooling (case B only) produced very limited crystallisation, with the measured crystallised area fraction increasing only from 5.3% to 13.2% between 5 and 40 min. The extracted kinetics ($k = 0.0152\ min^{-0.5}$; $t_{50} \approx 2079$ min) demonstrate that, in the present configuration, the cooling intensity and/or thermal contact were insufficient to initiate rapid crystallisation.

8. Electrode triggering (4.5 V, 1 min) produced minimal crystallisation at 30 °C, reaching only 9.0% at 40 min (case A). Under case B, crystallisation accelerated markedly and reached 95.5% at 40 min, with the fitted kinetic parameter increasing by ~15.6× (from $k = 0.2216$ to $0.4405\ min^{-0.5}$) and t_{50} decreasing from 1574 min to 6.49 min, confirming strong temperature-dependent enhancement for this trigger.

9. Mechanical agitation provided the strongest overall performance among the methods tested, delivering high crystallised fractions even at 30 °C (72.8% at 40 min, case A) and near-complete conversion at 60 °C (99.1% at 40 min, case B). The fitted kinetics increased from $k = 0.03185$ to $0.2157\ min^{-0.5}$, with the computed t_{50} decreasing from 9.79 min to 2.47 min, demonstrating that agitation is rapid even without pre-heating and becomes fastest under case B.

LIMITATIONS AND FUTURE DIRECTIONS

A key limitation of the present work lies in the crystallisation observation method. The growth of the solid phase was monitored using video recording and subsequent frame-by-frame screenshots, which were then processed to estimate the crystallised area. Nevertheless, this approach is useful for providing an overall visual and quantitative overview of the crystallisation patterns, but the temporal resolution is constrained by the frame rate and manual frame selection, and only a 2D projection of the crystallised region is captured rather than the full three-dimensional volume. In addition, the method does not directly resolve local temperature gradients or the detailed thermal field inside the PCM during crystallisation, so the coupling between heat release and front propagation is inferred indirectly.

Avrami-type relations are widely used to study PCM crystallisation but have not been specifically applied to the binary polyols examined. Note that, Avrami-type correlations, originally derived for isothermal conditions, are used only as an empirical reference for comparing crystallisation responses. The model is not intended to capture full non-isothermal thermodynamic coupling, but to provide a consistent phenomenological basis for comparing different triggering mechanisms, including cases with and without cold crystallisation during heating. Therefore, in this study, the Avrami exponent n was fixed at 0.5 to allow fair comparison between different triggering mechanisms. A more detailed analysis is still needed to rigorously test how well Avrami kinetics match the triggering behaviour of individual polyols.

Future work will then be focusing on refining both the measurement techniques and the understanding of mechanically induced crystallisation. For mechanical agitation in particular, more detailed thermal measurements are needed, for example by combining embedded thermocouples or infrared thermography with in-situ visualisation to resolve the temperature evolution during cold crystallisation. The use of high-speed cameras would allow more accurate tracking of nucleation events and early-stage front propagation, reducing uncertainty in the kinetic fits and enabling the application of higher-order or spatially resolved models. Further studies could also investigate the influence of agitation intensity, geometry and frequency on crystallisation kinetics, as well as scale-up effects in larger volumes or different container configurations. The present findings are, however, sufficient for the main aim of this work, which is to identify promising binary mixtures and practical triggering methods for controllable supercooled PCMs.

ACKNOWLEDGMENTS

This research is funded by UKRI for Marie Skłodowska-Curie Actions (MSCA) Postdoctoral Fellowship Guarantee Funding (Ref: 101151868).

AUTHOR CONTRIBUTIONS

Hasila Jarimi: Writing – original draft, funding acquisition, conceptualisation, experimentation, analysis.

Ze Liu: Writing – review & editing. **Yuehong Su**: Project management, supervision, writing – review & editing.

COMPETING INTERESTS

The authors declare that they have no known competing financial interests or personal relationships that could have appeared to influence the work reported in this paper.

DATA ACCESSIBILITY

The datasets generated and/or analysed during the current study are available from the corresponding author upon reasonable request.

REFERENCES

Aladool, A., Aziz, M. M., & Wright, C. D., 2017. Understanding the importance of the temperature dependence of viscosity on the crystallization dynamics in the Ge2Sb2Te5 phase-change material. Journal of Applied Physics, 121(22). DOI: https://doi.org/10.1063/1.4985282.

Avrami, M., 1940. Kinetics of Phase Change. II Transformation-Time Relations for Random Distribution of Nuclei. The Journal of Chemical Physics, 8(2), 212–224. DOI: https://doi.org/10.1063/1.1750631.

Avrami, M., 1941. Granulation, Phase Change, and Microstructure Kinetics of Phase Change. III. The Journal of Chemical Physics, 9(2), 177–184. DOI: https://doi.org/10.1063/1.1750872.

Beaupere, N., Soupremanien, U., & Zalewski, L., 2018. Nucleation triggering methods in supercooled phase change materials (PCM), a review. In Thermochimica Acta (Vol. 670, pp. 184–201). Elsevier B.V. DOI: https://doi.org/10.1016/j.tca.2018.10.009.

Callister Jr, W. D., & Rethwisch, D. G., 2020. Materials science and engineering: an introduction. John wiley & sons.

Chen, W., Chen, L., Li, L., Dong, C., & Zhang, L., 2023. Electrically-triggered nucleation of supercooled sodium acetate trihydrate phase change composites. Chemical Engineering Journal, 456. DOI: https://doi.org/10.1016/j.cej.2022.141131.

Dong, C., Jia, S., Lu, F., Wu, S., & Chen, W., 2024. Experimental study on the electrically-triggered crystallization behavior of supercooled copper foam-based and expanded graphite-based sodium acetate trihydrate. Solar Energy Materials and Solar Cells, 269. DOI: https://doi.org/10.1016/j.solmat.2024.112766.

Englmair, G., Jiang, Y., Dannemand, M., Moser, C., Schranzhofer, H., Furbo, S., & Fan, J., 2018. Crystallization by local cooling of supercooled sodium acetate trihydrate composites for long-term heat storage. Energy and Buildings, 180, 159–171. DOI: https://doi.org/10.1016/j.enbuild.2018.09.035.

Englmair, G., Moser, C., Furbo, S., Dannemand, M., & Fan, J., 2018. Design and functionality of a segmented heat-storage prototype utilizing stable supercooling of sodium acetate trihydrate in a solar heating system. Applied Energy, 221, 522–534. DOI: https://doi.org/10.1016/j.apenergy.2018.03.124.

Fan, C., Yuan, G., Wang, Y., Zhang, Y., & Wang, Z., 2022. Thermal storage performance of eutectic sugar alcohols applied to buildings and enhancement of crystallization. Solar Energy, 234, 231–239. DOI: https://doi.org/https://doi.org/10.1016/j.solener.2022.01.069.

Hou, X., Gao, Y., Xing, Y., Xu, Z., Yin, J., & Wang, S., 2023. Bubble-injection and seeding enabled crystallization of erythritol/xylitol eutectic phase change material. Case Studies in Thermal Engineering, 49. DOI: https://doi.org/10.1016/j.csite.2023.103278.

Hozumi, T., Saito, A., Okawa, S., & Matsui, T. (n.d.). Freezing phenomena of supercooled water under impacts of ultrasonic waves. Retrieved www.elsevier.com/locate/ijrefrig.

Jarimi, H., Devrim, A., Su, Y., & Riffat, S., 2025. Controllable Supercooling in Phase Change Materials-Advances in Triggering Methods, Lab-Scale Investigations, and Prototype Demonstrations. Journal of Global Decarbonisation, 1(Volume 2025, Number 1), 1–25. DOI: https://doi.org/10.17184/eac.9501.

Jarimi, H., Su, Y., & Riffat, S., 2026. Assessing the potential of binary and ternary supercooled sugar alcohol-based PCMs as a thermal battery. Applied Thermal Engineering, 292, 130268. DOI: https://doi.org/10.1016/j.applthermaleng.2026.130268.

Johnson, W. A., 1939. Reaction kinetics in process of nucleation and growth. Transactions of the American Institute of Mining and Metallurgical Engineers, 135, 416–458.

Kalidasan, B., Pandey, A. K., Saidur, R., Tyagi, S. K., & Mishra, Y. K., 2023. Experimental evaluation of binary and ternary eutectic phase change material for sustainable thermal energy storage. Journal of Energy Storage, 68. DOI: https://doi.org/10.1016/j.est.2023.107707.

Karthika, S., Radhakrishnan, T. K., & Kalaichelvi, P., 2016. A Review of Classical and Nonclassical Nucleation Theories.

Crystal Growth & Design, 16(11), 6663–6681. DOI: https://doi.org/10.1021/acs.cgd.6b00794.

Kutlu, C., Su, Y., Lyu, Q., & Riffat, S., 2023. Thermal management of using crystallization-controllable supercooled PCM in space heating applications for different heating profiles in the UK. Renewable Energy, 206, 848–857. DOI: https://doi.org/10.1016/j.renene.2023.02.077.

Lv, L., Huang, S., Cen, K., & Zhou, H., 2023. Experimental study of screening polyols and their binary eutectic phase change materials for long-term thermal energy storage. Journal of Cleaner Production, 399. DOI: https://doi.org/10.1016/j.jclepro.2023.136636.

Nomura, T., Zhu, C., Sagara, A., Okinaka, N., & Akiyama, T., 2015. Estimation of thermal endurance of multicomponent sugar alcohols as phase change materials. Applied Thermal Engineering, 75, 481–486. DOI: https://doi.org/10.1016/j.applthermaleng.2014.09.032.

Palomo Del Barrio, E., Cadoret, R., Daranlot, J., & Achchaq, F., 2016. New sugar alcohols mixtures for long-term thermal energy storage applications at temperatures between 70 °C and 100 °C. Solar Energy Materials and Solar Cells, 155, 454–468. DOI: https://doi.org/10.1016/j.solmat.2016.06.048.

Paul, A., Shi, L., & Bielawski, C. W., 2015. A eutectic mixture of galactitol and mannitol as a phase change material for latent heat storage. Energy Conversion and Management, 103, 139–146. DOI: https://doi.org/10.1016/j.enconman.2015.06.013.

Puupponen, S., & Seppälä, A., 2018. Cold-crystallization of polyelectrolyte absorbed polyol for long-term thermal energy storage. Sol. Energy Mater. Sol. Cells, 180. DOI: https://doi.org/10.1016/j.solmat.2018.02.013.

Sandnes, B., & Rekstad, J., 2006. Supercooling salt hydrates: Stored enthalpy as a function of temperature. Solar Energy, 80(5), 616–625. DOI: https://doi.org/10.1016/j.solener.2004.11.014.

Shao, X., 2018. Screening of sugar alcohols and their binary eutectic mixtures as phase change materials for low-to-medium temperature latent heat storage. (I): Non-isothermal melting and crystallization behaviors. Energy, 160. DOI: https://doi.org/10.1016/j.energy.2018.07.081.

Shao, X., Chenxu, Y., Wang, B., Zhang, N., & Yuan, Y., 2023. Mechanical agitation triggered crystallization of eutectic phase change material xylitol/erythritol with persistent supercooling for controllable heat retrieval. Solar Energy Materials and Solar Cells, 256. DOI: https://doi.org/10.1016/j.solmat.2023.112335.

Shao, X., Yang, S., Fan, L., & Yuan, Y., 2023. Sugar alcohol phase change materials for low-to-medium temperature thermal energy storage: a comprehensive review. J. Energy Storage, 68. DOI: https://doi.org/10.1016/j.est.2023.107848.

Shirzad, K., & Viney, C., 2023. A critical review on applications of the Avrami equation beyond materials science. Journal of The Royal Society Interface, 20(203), 20230242. DOI: https://doi.org/10.1098/rsif.2023.0242.

Sosso, G. C., Chen, J., Cox, S. J., Fitzner, M., Pedevilla, P., Zen, A., & Michaelides, A., 2016. Crystal Nucleation in Liquids: Open Questions and Future Challenges in Molecular Dynamics Simulations. Chemical Reviews, 116(12), 7078–7116. DOI: https://doi.org/10.1021/acs.chemrev.5b00744.

Turunen, K., Mikkola, V., Laukkanen, T., & Seppälä, A., 2023. Long-term thermal energy storage prototype of cold-crystallizing erythritol-polyelectrolyte. Applied Energy, 332. DOI: https://doi.org/10.1016/j.apenergy.2022.120530.

Turunen, K., Yazdani, M. R., Santasalo-Aarnio, A., & Seppälä, A., 2021. Exceptional cold-crystallization kinetics of erythritol-polyelectrolyte enables long-term thermal energy storage. Solar Energy Materials and Solar Cells, 230. DOI: https://doi.org/10.1016/j.solmat.2021.111273.

Xi, S., Wang, L., Xie, H., & Yu, W., 2022. Superhydrophilic Modified Elastomeric RGO Aerogel Based Hydrated Salt Phase Change Materials for Effective Solar Thermal Conversion and Storage. ACS Nano, 16(3), 3843–3851. DOI: https://doi.org/10.1021/acsnano.1c08581.

Xu, X., Dong, Z., Memon, S. A., Bao, X., & Cui, H., 2017. Preparation and supercooling modification of salt hydrate phase change materials based on $CaCl_2 \cdot 2H_2O/CaCl_2$. Materials, 10(7). DOI: https://doi.org/10.3390/ma10070691.

Yang, S., Shao, X. F., Shi, H. Y., Luo, J. H., & Fan, L. W., 2022. Bubble-injection-enabled significant reduction of supercooling and controllable triggering of crystallization of erythritol for medium-temperature thermal energy storage. Solar Energy Materials and Solar Cells, 236. DOI: https://doi.org/10.1016/j.solmat.2021.111538.

Yuan, M., Xu, C., Wang, T., Zhang, T., Pan, X., & Ye, F., 2021. Supercooling suppression and crystallization behaviour of erythritol/expanded graphite as form-stable phase change material. Chemical Engineering Journal, 413. DOI: https://doi.org/10.1016/j.cej.2020.127394.

Zhou, G., Zhu, M., & Xiang, Y., 2018. Effect of percussion vibration on solidification of supercooled salt hydrate PCM in thermal storage unit. Renewable Energy, 126, 537–544. DOI: https://doi.org/10.1016/j.renene.2018.03.077.